SeV/GDNF and SeV/NGF were injected 4 h after ischemia. Surviving neurons in the hippocampal CA1 region were observed in gerbils treated with either SeV/ GDNF or SeV/NGF, although a few degenerated nuclei of neurons were observed in these cases (Figure 5b, c). The number of surviving neurons in the hippocampal CA1 region was also counted (Figure 6). Administration of SeV/GDNF (114.7±9.7 cells/mm) or SeV/NGF (127.6±13.8 cells/mm) prevented the neuronal death as compared to administration of SeV/GFP (14.3±5.6 cells/ mm) ($P<0.01$), even if the vectors were administered 4 h after ischemia. Moreover, treatment with SeV/GDNF (74.2±9.6 cells/mm) or SeV/NGF (76.4±10.8 cells/mm) 6 h after ischemic insult was also effective for prevention of the delayed neuronal death as compared to treatment with SeV/GFP (11.7±2.3 cells/mm) ($P<0.01$) (Figure 5e, f and Figure 6). Equal neuroprotective effects were observed on the ipsilateral and contralateral sides of the hippocampal CA1 region (data not shown), indicating that the proteins expressed by SeV vectors were extensively dispersed. These results indicate that administration of SeV/GDNF or SeV/NGF even several hours after ischemia effectively prevents the delayed neuronal death induced by transient global ischemia. There have been no previous reports showing that the administration of virus vector-mediated genes at 4 h or even 6 h after an ischemic insult was effective for preventing the delayed neuronal death induced by transient ischemia in animal models. Our results indicate that the time window for the treatment of cerebral ischemia could be substantially extended. It was reported that more than 8 h was required for the expression of genes carried by adenovirus vectors in the rat brain.[34] Thus, the time needed for expression of genes carried by SeV vector

may be shorter than that needed for genes carried by adenovirus vector. The rapid gene expression achieved using SeV vectors may be due to the rapid replication, high level of mRNA transcription and effective translation of the mRNA of the vectors, that is, the typical features of RNA viruses. This may have led to the protective effect observed even with 6 h postischemic administration of SeV vectors against the delayed
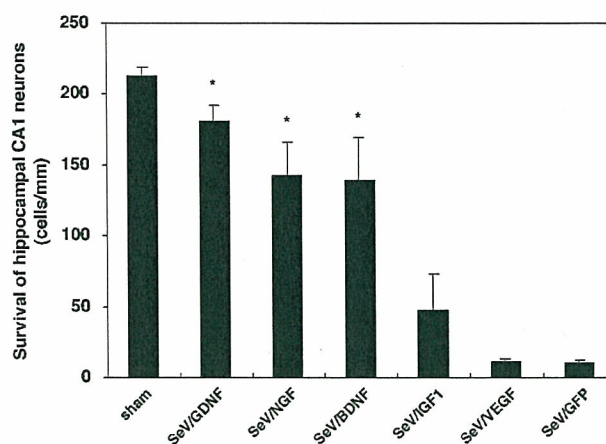

Figure 4 Quantitative analysis of the effect of SeV vector on ischemic injury when administered 30 min after ischemia. SeV/GDNF, SeV/NGF, SeV/BDNF, SeV/IGF-1, SeV/VEGF or SeV/GFP was injected intraventricularly 30 min after ischemic insult. The number of surviving neurons/ 1-mm length in the hippocampal CA1 region was calculated. Values are expressed as the mean±s.d. (n = 8 animals per group). Asterisks indicate a significant difference as compared with the SeV/GFP-treated group. ($P<0.01$, Student's t test).
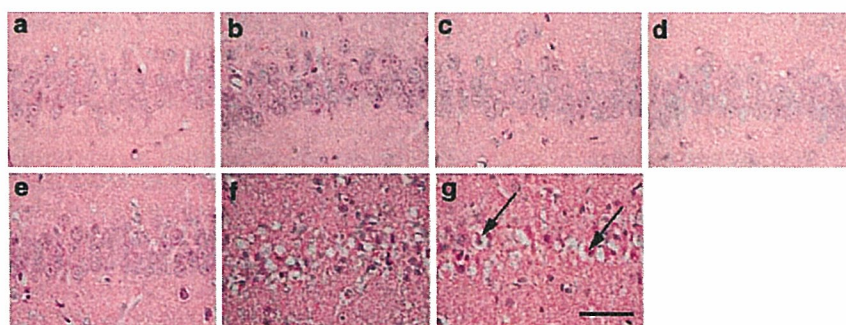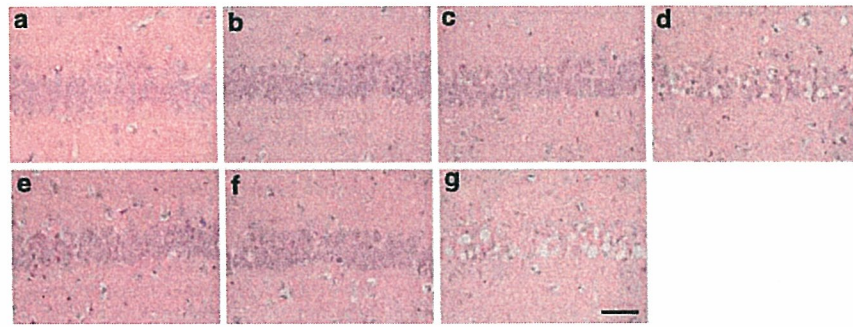

Figure 3 Representative photographs of pyramidal neurons in the hippocampal CA1 region after treatment (30 min after ischemia) with SeV vector following ischemic injury. (a) Sham-operated gerbils; (b) SeV/GDNF-, (c) SeV/NGF- (d) SeV/BDNF-, (e) SeV/IGF-1-, (f) SeV/VEGF- and (g) SeV/GFP-treated gerbils 30 min after ischemic insult. These sections were stained with hematoxylin and eosin. Arrows indicate the pyknotic nuclei of neurons. Scale bar = 50 μm. SeV vectors carrying the BDNF (SeV/BDNF), IGF-1 (SeV/IGF-1) and VEGF (SeV/VEGF) genes were constructed as described in Figure 1. In this experiment, human BDNF (accession number: XM_006027), human IGF-1 (accession number: X56773) and human VEGF (accession number: AY047581) cDNAs were amplified with a pair of NotI-tagged (underlined) primers containing SeV-specific transcriptional regulatory signal sequences, 5'-ACTTGCGGCCGCCAAAGTTCAGTGATGACCATCCTTTTCCTTAC-3' and 5'-ATCCGCGGCCGCGATGAACTTTCACCCTAAGTTTTTCTTAC TACGGCTATCTTCCCCTTTTAATGGTCAATGTAC-3' for BDNF, 5'-ACTTGCGGCCGCCAAAGTTCAGCAATGGGAAAAATCAGCAGTCTTC-3' and 5'-ATCCGCGGCCGCGATGAACTTTCACCCTAAGTTTTTCTTACTACGGCTACATCCTGTAGTTCTTGTTTCCTGC-3' for IGF-1 and 5'-ACTTGCGGCCGCCAAAGTTCACTAATGAACTTTCTGCTGTCTTGGGTGC-3' and 5'-ATCCGCGGCCGCGATGAACTTTCACCC TAAGTTTTTCTTACTACGGTCACCGCCTCGGCTTGTCACATCTGC-3' for VEGF. Adult male Mongolian gerbils (60–80 g) were used in this experiment. Occlusion of the bilateral common carotid arteries was performed as previously described.[19,27] Briefly, gerbils were anesthetized by an intraperitoneal injection of chloral hydrate (300 mg/kg)[19] and both common carotid arteries were clamped for 5 min with surgical clips to produce transient forebrain ischemia. The body temperature was measured using a thermocouple probe inserted into the anus and maintained at 37.5°C using a heating pad. Sham-operated animals were treated in the same manner except for occlusion of the bilateral common carotid arteries. At 30 min after the ischemic insults, SeV/GDNF, SeV/NGF, SeV/BDNF, SeV/IGF-1, SeV/VEGF or SeV/GFP (5 × 10^6 PFU/head, n = 8 animals per group) was injected intraventricularly into gerbils. At 6 days after injection, the gerbils were anesthetized with ether and transcardially perfused with normal saline followed by 4% paraformaldehyde in 0.1 M phosphate buffer (PB). The brains were removed and fixed in the same fixative overnight and then processed into paraffin blocks. Coronal brain sections were cut at 5-μm thickness and stained with hematoxylin and eosin. Arrows indicate the pyknotic nuclei of neurons. Scale bar = 50 μm.

Figure 5 Representative photographs of pyramidal neurons in the hippocampal CA1 regions after treatment (4 and 6 h after ischemia) with SeV vector following ischemic injury. SeV/GDNF (b, e), SeV/NGF (c, f) or SeV/GFP (d, g) was administered intraventricularly 4 h (b, c, d) or 6 h (e, f, g) after ischemic insult. The sections were stained with hematoxylin and eosin. Scale bar = 50 μm. Occlusion of the bilateral common carotid arteries was performed as described in Figure 2.

neuronal death of the hippocampal CA1 pyramidal neurons induced by transient ischemia. Moreover, these attractive features of SeV vectors may make them useful for the treatment of acute diseases such as cerebral ischemia.

It has been reported that NGF administration prevented the delayed neuronal death when neurons were observed 7 days after ischemic insult, but not when they were observed 28 days after the insult.[18] The long-term effects of the vectors studied here therefore had to be examined to better clarify their potential benefits in clinical use. Therefore, we also examined the long-term effects of SeV/GDNF and SeV/NGF on delayed neuronal death. The effect of SeV vectors for preventing neuronal death could be observed even when analyzed 28 days after the insult, although it was not seen in the case of topical application of NGF protein.[18] However, the number of surviving neurons at 28 days after the ischemia was reduced to almost half of that at 6 days after ischemia in the cases of gerbils treated with SeV/GDNF and SeV/NGF (Figure 7). High-level expression of the vector-encoded protein was detected after the administration of the SeV vector, but this expression reached a peak 4 days after the administration and then decreased to the basal level by 14 days. It is probable that immune responses induced by the virus particles or genes derived from SeV may cause the rapid decline of the gene expression of SeV. However, this limitation may be circumvented by the development of a new generation of SeV vectors that elicit weaker immune responses, which should extend the duration of gene expression. We have developed a series of an attenuated type of SeV vectors that are F gene-deleted,[24] F gene-deleted with preferable mutations,[35] M gene-deleted,[36] or have combinations of deletions of these genes (Kitazato K, unpublished; Inoue M, unpublished). We plan the first clinical application of SeV vector carrying human fibroblast growth factor-2 for the treatment of peripheral arterial disease using F gene-deleted SeV vector. As the F gene-deleted SeV is nontransmissible and shows less cytopathic effect than the wild-type SeV, we should utilize this type of SeV (or further advanced types of SeV vector) for applications to brain ischemia. Improvement of the vector modifications will ultimately provide better protection against ischemic injury. Moreover, alternative administration routes, such as lumbar puncture of the vectors, should be developed for the purposes of human
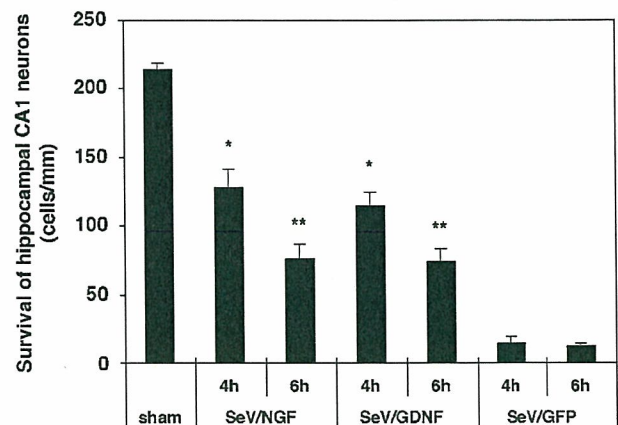
Figure 6 Quantitative analysis of the effect of SeV vector on ischemic injury when administered 4 and 6 h after ischemia. SeV/GDNF, SeV/NGF or SeV/GFP was injected intraventricularly 4 or 6 h after ischemic insult. The number of surviving neurons/1-mm length in the hippocampal CA1 region was calculated. Values are expressed as the mean±s.d. (n = 8 animals per group). Asterisks indicate a significant difference as compared with the SeV/GFP-treated group. (P < 0.01, Student's t test).

gene therapy for cerebrovascular diseases. Hayashi and co-workers[37] reported that liposome-mediated hepatocyte growth factor (HGF) gene transfer into the subarachnoid space prevented delayed neuronal death in gerbils. Intrathecal injection into the cisterna magna involves no systematic anesthesia, no burr hole and no pain for patients. For use in clinical application, these methods should be tested in future studies. More importantly, we have already confirmed the efficient replication of SeV vectors in primates. In fact, high-level expression of GDNF (more than 100 ng/ml) was observed in cerebrospinal fluid after the injection of SeV vector carrying the GDNF gene (SeV/GDNF) into the lateral ventricle of primates (data not shown). Thus, we are going to evaluate the SeV/GDNF vector for its effects on the recovery from brain ischemia using primates. In such experiments, we hope to show a correlation between CA1 neuroprotection and functional recovery.

In conclusion, the present study demonstrated that postischemic administration of SeV vectors carrying genes for GDNF and NGF effectively prevented the delayed neuronal death of the hippocampal CA1
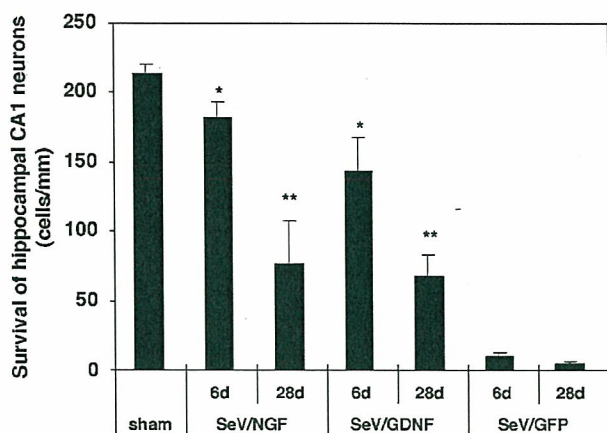
Figure 7 Long-term effect of the SeV vectors on ischemic injury. SeV/GDNF, SeV/NGF or SeV/GFP was injected intraventricularly 30 min after ischemic insult. At 6 days or 28 days after injection, gerbils were anesthetized, and the number of surviving neurons/1-mm length in the hippocampal CA1 region was calculated. Values are expressed as the mean±s.d. (n = 8 animals per group). Asterisks indicate a significant difference as compared with the SeV/GFP-treated group. (P < 0.01, Student's t test).

pyramidal cells induced by occlusion of the bilateral carotid arteries. It is noteworthy that the neuroprotective effect was obtained even 4 and 6 h after ischemic insults. These results indicate that gene therapy using SeV vectors is of great potential usefulness for the treatment of cerebral ischemia.

Acknowledgements

References

1 Kirino T. Delayed neuronal death in the gerbil hippocampus following ischemia. *Brain Res* 1982; **239**: 57–59.

2 Kirino T, Sano K. Selective vulnerability in the gerbil hippocampus following transient ischemia. *Acta Neuropathol (Berl.)* 1984; **62**: 201–208.

3 Andersen MB, Sams-Dodd F. Impairment of working memory in the T-maze after transient global cerebral ischemia in the Mongolian gerbil. *Behav Brain Res* 1998; **91**: 15–22.

4 Li AJ et al. Protective effect of acidic fibroblast growth factor against ischemia-induced learning and memory deficits in two tasks in gerbils. *Physiol Behav* 1999; **66**: 577–583.

5 Catania MA et al. Erythropoietin prevents cognition impairment induced by transient brain ischemia in gerbils. *Eur J Pharmacol* 2002; **437**: 147–150.

6 Beck KD et al. Mesencephalic dopaminergic neurons protected by GDNF from axotomy-induced degeneration in the adult brain. *Nature* 1995; **373**: 339–341.

7 Choi-Lundberg DL et al. Dopaminergic neurons protected from degeneration by GDNF gene therapy. *Science* 1997; **275**: 838–841.

8 Henderson CE et al. GDNF: a potent survival factor for motoneurons present in peripheral nerve and muscle. *Science* 1994; **266**: 1062–1064.

9 Li L et al. Rescue of adult mouse motoneurons from injury-induced cell death by glial cell line-derived neurotrophic factor. *Proc Natl Acad Sci USA* 1995; **92**: 9771–9775.

10 Fischer W et al. Amelioration of cholinergic neuron atrophy and spatial memory impairment in aged rats by nerve growth factor. *Nature* 1987; **329**: 65–68.

11 Montero CN, Hefti F. Rescue of lesioned septal cholinergic neurons by nerve growth factor: specificity and requirement for chronic treatment. *J Neurosci* 1988; **8**: 2986–2999.

12 Tuszynski MH, U HS, Amaral DG, Gage FH. Nerve growth factor infusion in the primate brain reduces lesion-induced cholinergic neuronal degeneration. *J Neurosci* 1990; **10**: 3604–3614.

13 Abe K, Hayashi T, Itoyama Y. Amelioration of brain edema by topical application of glial cell line-derived neurotrophic factor in reperfused rat brain. *Neurosci Lett* 1997; **231**: 37–40.

14 Kitagawa H et al. Reduction of ischemic brain injury by topical application of glial cell line-derived neurotrophic factor after permanent middle cerebral artery occlusion in rats. *Stroke* 1998; **29**: 1417–1422.

15 Miyazaki H et al. Glial cell line-derived neurotrophic factor protects against delayed neuronal death after transient forebrain ischemia in rats. *Neuroscience* 1999; **89**: 643–647.

16 Shigeno T et al. Amelioration of delayed neuronal death in the hippocampus by nerve growth factor. *J Neurosci* 1991; **11**: 2914–2919.

17 Yamamoto S et al. Protective effect of NGF atelocollagen mini-pellet on the hippocampal delayed neuronal death in gerbils. *Neurosci Lett* 1992; **141**: 161–165.

18 Ishimaru H et al. NGF delays rather than prevents the cholinergic terminal damage and delayed neuronal death in the hippocampus after ischemia. *Brain Res* 1998; **789**: 194–200.

19 Yagi T et al. Rescue of ischemic brain injury by adenoviral gene transfer of glial cell line-derived neurotrophic factor after transient global ischemia in gerbils. *Brain Res* 2000; **885**: 273–282.

20 Hermann DM et al. Adenovirus-mediated GDNF and CNTF pretreatment protects against striatal injury following transient middle cerebral artery occlusion in mice. *Neurobiol Dis* 2001; **8**: 655–666.

21 Andsberg G et al. Neuropathological and behavioral consequences of adeno-associated viral vector-mediated continuous intrastriatal neurotrophin delivery in a focal ischemia model in rats. *Neurobiol Dis* 2002; **9**: 187–204.

22 Lamb RA, Kolakofsky D. Paramyxoviridae: the virus and their replication. In: Fields BN, Knipe DM, Howley PM (eds) *Fields Virology*. Lippincott-Raven: Philadelphia, 1996, pp. 1177–1204.

23 Nagai Y, Kato A. Paramyxovirus reverses genetics is coming of age. *Microbiol Immunol* 1999; **43**: 613–624.

24 Li HO et al. A cytoplasmic RNA vector derived from non-transmissible Sendai virus with efficient gene transfer and expression. *J Virol* 2000; **74**: 6564–6569.

25 Yonemitsu Y et al. Efficient gene transfer to airway epithelium using recombinant Sendai virus. *Nat Biotechnol* 2000; **18**: 970–973.

26 Shiotani A et al. Skeletal muscle regeneration after insulin-like growth factor I gene transfer by recombinant Sendai virus vector. *Gene Therapy* 2001; **8**: 1043–1050.

27 Shirakura M et al. Sendai virus vector-mediated gene transfer of glial cell line-derived neurotrophic factor prevents delayed neuronal death after transient global ischemia in gerbils. *Exp Anim* 2003; **52**: 119–127.

28 Kato A et al. Initiation of Sendai virus multiplication from transfected cDNA or RNA with negative or positive sense. *Genes Cells* 1996; **1**: 569–579.

29 Kitagawa H et al. Adenovirus-mediated gene transfer of glial cell line-derived neurotrophic factor prevents ischemic brain injury after transient middle cerebral artery occlusion in rats. *J Cereb Blood Flow Metab* 1999; **19**: 1336–1344.

Calcium-permeable AMPA receptors promote misfolding of mutant SOD1 protein and development of amyotrophic lateral sclerosis in a transgenic mouse model

Minako Tateno[1], Hisako Sadakata[1], Mika Tanaka[2], Shigeyoshi Itohara[2], Ryong-Moon Shin[3], Masami Miura[3], Masao Masuda[3], Toshihiko Aosaki[3], Makoto Urushitani[1], Hidemi Misawa[4] and Ryosuke Takahashi[1,*]

[1]Laboratory for Motor System Neurodegeneration and [2]Laboratory for Behavioral Genetics, Brain Science Institute, RIKEN, Wako, Saitama 351-0198, Japan, [3]Neural Circuits Dynamics Research Group, Tokyo Metropolitan Institute of Gerontology, Itabashi, Tokyo 173-0015, Japan and [4]Department of Neurology, Tokyo Metropolitan Institute for Neuroscience, Fuchu, Tokyo 183-8526, Japan

Mutant Cu/Zn-superoxide dismutase (SOD1) protein aggregation has been suggested as responsible for amyotrophic lateral sclerosis (ALS), although the operative mediating factors are as yet unestablished. To evaluate the contribution of motoneuronal Ca^{2+}-permeable (GluR2 subunit-lacking) α-amino-3-hydroxy-5-methyl-4-isoxazole propionic acid (AMPA)-type glutamate receptors to SOD1-related motoneuronal death, we generated *chat-GluR2* transgenic mice with significantly reduced Ca^{2+}-permeability of these receptors in spinal motoneurons. Crossbreeding of the *hSOD1*[G93A] transgenic mouse model of ALS with *chat-GluR2* mice led to marked delay of disease onset (19.5%), mortality (14.3%) and the pathological hallmarks such as release of cytochrome *c* from mitochondria, induction of *cox2* and astrogliosis. Subcellular fractionation analysis revealed that unusual SOD1 species first accumulated in two fractions dense with neurofilaments/glial fibrillary acidic protein/nuclei and mitochondria long time before disease onset, and then concentrated into the former fraction by disease onset. All these processes for unusual SOD1 accumulation were considerably delayed by GluR2 overexpression. Ca^{2+}-influx through atypical motoneuronal AMPA receptors thus promotes a misfolding of mutant SOD1 protein and eventual death of these neurons.

INTRODUCTION

Amyotrophic lateral sclerosis (ALS) is a fatal, adult-onset neurodegenerative disease characterized by a selective loss of motoneurons in the spinal cord and brainstem (1). Mutation of Cu/Zn-superoxide dismutase (SOD1) is the most frequent cause of familial ALS (2). Introduction of such mutated SOD1 genes into mice causes ALS-like symptoms characterized by the selective death of spinal motoneurons, despite a ubiquitous expression of mutant proteins (3). Several lines of evidence have demonstrated that mutant SOD1 toxicity is not essentially due to decreased dismutase activity, but rather to a 'gain of toxic function' (4). This so-called 'oligomerization hypothesis' has recently attracted attention from ALS researchers. The hypothesis maintains that mutant SOD1 proteins are misfolded, and consequently oligomerized and aggregated, gaining toxic properties at some stage in their formation (5). The hypothesis is based on the numerous observations that SOD1-containing inclusions/high-molecular-weight-shifted protein complexes are specifically found in spinal motoneurons and their surrounding astrocytes from autopsied patients and transgenic mice carrying mutant SOD1 genes (6–8), in spinal cord extracts from mutant SOD1 transgenic mice (9–12) and in cultured motoneurons into which mutant SOD1 has been microinjected (13).

*To whom correspondence should be addressed at: Laboratory for Motor System Neurodegeneration, Brain Science Institute, Riken, 2-1 Hirosawa, Wako, Saitama 351-0198, Japan. Tel: +81 484676072; Fax: +81 484624796; Email: ryosuke@brain.riken.jp

However, in addition to this line of evidence, glutamate-induced excitotoxicity has also been implicated in the pathophysiology of ALS patients and mutant SOD1 transgenic mice (14–17). Pharmacological experiments have strongly suggested that the excitotoxicity of spinal motoneurons largely depends on Ca^{2+}-permeable α-amino-3-hydroxy-5-methyl-4-isoxazole propionic acid (AMPA) receptors specifically expressed in a subset of neurons, including spinal motoneurons (18,19). AMPA receptors, major mediators for fast excitatory neurotransmission in the mammalian central nervous system, are composed of a heteromeric complex of four subunits GluR1–GluR4, and the absence of GluR2 renders the receptor Ca^{2+}-permeable (20). As this unique property of GluR2 is generated posttranscriptionally by RNA editing, an editing failure can also produce Ca^{2+}-permeable AMPA receptors (21). Reduced editing efficiency of GluR2 mRNA has been specifically reported in spinal motoneurons from human sporadic ALS patients (22), further suggesting that Ca^{2+}-permeable AMPA receptor-mediated excitotoxicity is closely linked to the vulnerability of spinal motoneurons in ALS. However, whether and in what manner this atypical type of AMPA receptor affects mutant SOD1-induced motoneuronal degeneration remains to be elucidated.

The purpose of the present study was to explore a mechanistic link between glutamate toxicity and the conversion of mutant SOD1 into aberrant forms by modification of the electrophysiological properties of motoneuronal AMPA receptors in an ALS mouse model. The *chat-GluR2* transgenic mouse line was generated to overexpress *GluR2* in a cholinergic neuron-specific manner, resulting in a large reduction in Ca^{2+}-permeability of motoneuronal AMPA receptors. We detected various types of abnormally folded SOD1 proteins in fractions derived from different cellular compartments from *hSOD1*^{G93A} mice spinal cords. Double transgenic mice carrying both *chat-GluR2* and *hSOD1*^{G93A} displayed a marked delay of disease onset, followed by delayed formation of all the abnormal SOD1 species. These results indicate that Ca^{2+}-permeable AMPA receptors in motoneurons contribute to the conformational changes of mutant SOD1 and the subsequent neurodegeneration associated with these changes.

RESULTS

Generation and characterization of *chat-GluR2* transgenic mice: cholinergic neuron-specific GluR2 overexpression results in substantial reduction of Ca^{2+}-permeable AMPA receptors in spinal motoneurons

A mouse line with reduced numbers of Ca^{2+}-permeable AMPA receptors in spinal motoneurons was generated. Spinal motoneurons are typical cholinergic neurons, constituting a minor population among total spinal neurons. Thus, a cholinergic neuron-specific promoter, i.e. the choline acetyltransferase (*ChAT*) gene promoter (23) (Fig. 1A) was used to preferentially increase *GluR2* expression in spinal motoneurons. Three independent *chat-GluR2* transgenic lines, Tg3, Tg7 and Tg10, were established. To examine the copy number of the *chat-GluR2* transgene, Taqman quantitative DNA PCR and genomic Southern blotting were performed.

Results from Taqman PCR indicated that the Tg3, Tg7 and Tg10 lines contained ~2, 10 and 16 copies of the *chat-GluR2* transgene, respectively, a finding which was also supported by genomic Southern blotting (Fig. 1B). Expression patterns of the transgenes in the spinal cord were examined using *in situ* hybridization (Fig. 1C), revealing a preferential transcription of transgenes in cholinergic neurons in *chat-GluR2* mice. To quantify the *GluR2* mRNA level in spinal motoneurons, motoneurons were carefully purified from frozen slices of spinal cord using laser microdissection, because other neuronal populations such as dorsal horn neurons express high level of *GluR2*. Quantitative PCR analysis revealed that spinal motoneurons in Tg7 expressed levels of *GluR2* mRNA nearly 5-fold higher than those of non-transgenic control mice (Table 1). Tg10 included numerous copies of the transgene, but displayed lower levels of *GluR2* expression than Tg7, probably owing to DNA methylation of transgenes (data not shown). No significant changes in mRNA levels of *ChAT*, endogenous *SOD1*, *GluR3* or *GluR4* were observed in *chat-GluR2* transgenic mice compared with non-transgenic mice. Western blotting of the extracts prepared from the spinal cord ventral region also revealed a significant increase of the GluR2 protein level in Tg7 compared with that in non-transgenic littermates (Fig. 1D). *GluR2* expression was thus significantly increased in spinal motoneurons in *chat-GluR2* mice without affecting the expression of other AMPA receptor subunits. Next, the Ca^{2+}-permeability of AMPA receptors in spinal motoneurons was examined. Whole-cell patch-clamp recordings were performed on motoneurons in spinal cord slices. The first two graphs in Figure 1E represent typical I-V relationships, showing distinct inward rectification in wild-type (wt), whereas a linear relationship is seen in Tg7. Normalized I–V relationships reveal a clear difference between wt and Tg7 ($P < 0.001$). The rectification index, an index of Ca^{2+}-permeability calculated as the ratio of chord conductance at $+40$ and -70 mV, was estimated as 0.262 ± 0.024 for wt and 0.436 ± 0.038 for Tg7 (mean $\pm$ SEM, $P < 0.001$). Thus, the majority of AMPA receptors in spinal motoneurons were Ca^{2+}-impermeable in Tg7 mice, but were Ca^{2+}-permeable in non-transgenic controls.

Crossbreeding *hSOD1*^{G93A} transgenic mice with *chat-GluR2* transgenic mice markedly delays disease onset and mortality

The *chat-GluR2* transgenic mouse was mated with a *hSOD1*^{G93A} transgenic ALS mouse to generate double transgenic (GS) mice. Most of the spinal motoneuronal AMPA receptors were actually Ca^{2+}-impermeable in GS mice, but Ca^{2+}-permeable in littermates carrying only the *hSOD1*^{G93A} transgene (*S* mice, Fig. 2A). The G1L line of *hSOD1*^{G93A} mice develops overt symptoms defined as disease onset at around 7 months, a classification based on a sudden decrease in motor performance in behavioral tests such as the rotarod test (25,26). Death occurs at around 8.5–9 months. To evaluate the effects of reduced Ca^{2+}-permeability in AMPA receptors on the clinical course of ALS, motor performance was assessed by the rotarod test. Figure 2B depicts the rotarod score of each mouse measured every week, clearly showing that mice carrying the *SOD1*^{G93A} gene are rapidly declining
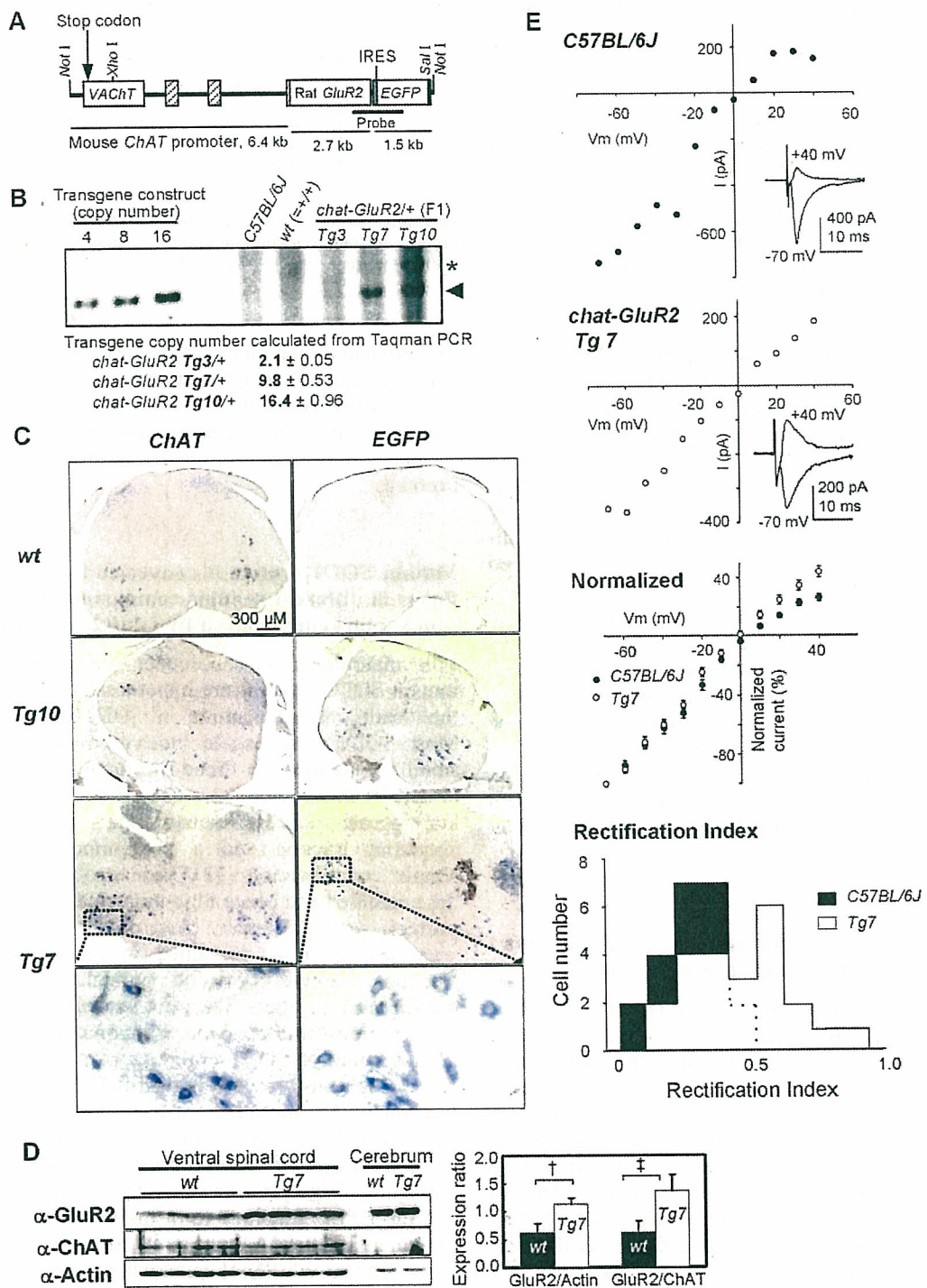
Figure 1. Generation and characterization of *chat-GluR2* transgenic mice. (**A**) The DNA fragment introduced into *chat-GluR2* transgenic mice contains the rat *GluR2* and *EGFP* coding sequences driven by mouse *ChAT* promoter. *GluR2* and *EGFP* are transcribed into the same mRNA, but are independently translated owing to the IRES. The striped and filled boxes represent exons of the endogenous *ChAT* gene and SV40 polyadenylation signal, respectively. (**B**) Transgene copy number was examined by genomic Southern blotting using the probe indicated in (A) (24) and by Taqman quantitative DNA PCR. The arrowhead indicates the *Xho* I–*Sal* I-digested 9.0 kb fragment of the transgene. (**C**) Transgene expression is predominant in cholinergic neurons. Either digoxigenin-labeled *EGFP* or *ChAT* riboprobe was used to hybridize to spinal cord sections. Both *EGFP* and *ChAT* were preferentially expressed in large cells (diameter ≥ 25 μm) located in the ventral horn, representing spinal motoneurons. (**D**) The GluR2 protein level is increased in the ventral half of the spinal cord in *chat-GluR2* transgenic mice. The ventral half was carefully dissected from T10–L5 segments of spinal cords. Extracts of ventral spinal cords (40 μg, $n = 4$) and cerebrum (10 μg, $n = 2$) were immunoblotted. † $P < 0.05$, ‡ $P < 0.01$. (**E**) The majority of AMPA receptors in spinal motoneurons were Ca^{2+}-impermeable in *chat-GluR2* transgenic mice. The excitatory postsynaptic potential (EPSC) of AMPA components was measured from 23 motoneurons of *chat-GluR2* transgenic mice (Tg7, $n = 11$) and 22 motoneurons of non-transgenic C57BL/6J mice (wt, $n = 9$), using the whole-cell patch-clamp method. Insets represent synaptic currents at holding potentials of −70 and +40 mV.

Table 1. GluR2 mRNA level is to increased in motoneurons of *chat-GluR2* transgenic mice

Mouse	GluR2	GluR3	GluR4	ChAT	SOD1
C57BL/6J ($n = 3$)	1.00	1.00	1.00	1.00	1.00
GluR2-Tg3 ($n = 3$)	0.96 ± 0.27	0.91 ± 0.13	1.23 ± 0.27	1.01 ± 0.16	0.74 ± 0.20
GluR2-Tg7 ($n = 3$)	4.78 ± 0.85*	1.02 ± 0.54	1.21 ± 0.26	1.17 ± 0.38	1.09 ± 0.41
GluR2-Tg10 ($n = 6$)	1.58 ± 0.38**	0.92 ± 0.92	1.22 ± 0.48	1.15 ± 0.58	1.02 ± 0.15

Motoneurons in spinal cord were collected using laser microdissection. Transcription levels of several genes were examined by Taqman real-time quantitative PCR. Data were normalized with *GAPDH* expression and then represent relative expression levels compared with levels in C57BL/6J non-transgenic control mice (mean ± SD). Not significantly different ($P > 0.05$) except for *($P = 0.0015$) and **($P = 0.0184$), compared with non-transgenic controls.

in performance score after a certain period. The day just before the decline in score was defined as the day of disease onset, and the mean time of disease onset was compared between S and GS littermates. Disease onset in GS mice was delayed, by 42.9 days (19.5%) in Tg7 and 18.7 days (8.5%) in Tg10, as compared with S mice. Lifespan was also prolonged in GS mice, by 37.5 days (14.3%) in Tg7 and 15.2 days (5.7%) in Tg10 (Fig. 2C, Table 2). No significant difference in rotarod score or lifespan was observed between the *chat-GluR2* and wt mice (data not shown). Furthermore, no prolongation of lifespan was observed in the GS mice generated from Tg3 (data not shown), which animals displayed no additional *GluR2* expression in spinal motoneurons (Table 1). The number of motoneurons in the spinal cord was counted, revealing that degeneration of motoneurons was also delayed in GS mice from the Tg7 line (Fig. 2D). All these results indicate that reducing Ca^{2+}-permeability in AMPA receptors delays disease onset and motoneuron death caused by mutant SOD1, presumably in a dose-dependent manner.

cytochrome *c*-release from mitochondria, *cox2*-induction and gliosis are delayed by GluR2 overexpression

We next investigated whether pathological changes related to disease onset are verifiably affected by overexpression of GluR2. Of the numerous events accompanying disease onset in $hSOD1^{G93A}$ mice, we focused on cytochrome *c*-release from mitochondria and induction of cyclooxygenase-2 (*cox-2*), as a treatment of $hSOD1^{G93A}$ mice with agents inhibiting these events delays disease onset (26,27). Cytochrome *c*, which is normally localized to the intermembrane space of mitochondria, activates caspases and subsequent apoptosis after release into the cytosol (28). Cox-2 catalyzes the synthesis of prostaglandin E2, which stimulates glutamate release from astrocytes and plays a key role in the inflammatory process (29). Cytosolic extracts (26) and RNA were prepared from the spinal cord lumbar region, as this is the most severely affected region in ALS. Cytochrome *c* became clearly detectable in the cytosolic fraction around 7 months in S, but was only faintly detectable even at 8 months in GS littermates, indicating that the release of cytochrome *c* is considerably delayed in GS mice (Fig. 3A). Induction of *cox-2* transcription was also significantly delayed in GS in comparison to S littermates (Fig. 3B). After disease onset, $hSOD1^{G93A}$ mice exhibit severe gliosis in the spinal cord owing to

exacerbated inflammation (30). We also found that astrogliosis was remarkably delayed in GS mice (Fig. 3C). Reducing Ca^{2+}-permeability of AMPA receptors is thus likely to affect the upstream events of cytochrome *c*-release and *cox-2* induction among the processes triggered by mutant SOD1 proteins.

Mutant SOD1 protein is converted into various unusual forms in different cellular compartments, but the conversion is markedly delayed by GluR2 overexpression

The misfolding and subsequent conformational changes in mutant SOD1 proteins are hypothesized to be responsible for the death of motoneurons in SOD1-related ALS (5,9,10). Most SOD1 proteins are located in the cytosol, but very small populations are found in organelles such as mitochondria (31) and nuclei (32). Therefore, we roughly divided a homogenate from the lumbar spinal cord into a crude mitochondrial fraction and a post-mitochondrial fraction by simple centrifugation (31), and analyzed in which fraction the misfolded and hence high-molecular-weight-shifted SOD1 proteins were detectable. Most organelles and cytoskeletons were found to be contained in the crude mitochondrial fraction, whereas cytosolic proteins were in the post-mitochondrial fraction (data not shown).

As the post-mitochondrial fraction contained an extremely large amount of SOD1 proteins, it was a formidable task to detect high-molecular-weight-shifted SOD1 species in this fraction by conventional western blotting (data not shown). To enhance the sensitivity of detection, the post-mitochondrial fraction was size-fractionated using size-exclusive chromatography with high-performance liquid chromatography (HPLC), and the HPLC fractions were immunoblotted. The results as shown in Figure 4A indicated that, in addition to the very large amount of SOD1 monomers, high-molecular-weight-shifted SOD1-immunopositive species corresponding to dimer (*2), trimer (*3) and tetramer (*4) sizes of mutant SOD1 were detectable in 2-, 6- and 8-month-old S mice, respectively (Fig. 4A). These oligomer-sized species were not observably detected in the lumbar spinal cord from wt or the cerebrum from S littermates even at 8 months, suggesting that the conversion of the SOD1 protein into oligomer-sized forms preferentially occurs in the spinal cord. The molecular shifts of those species were not due to ubiquitination, as they were not detected by anti-ubiquitin antibody (Supplementary Material, Fig. S1). Formation of oligomer-sized SOD1 aberrant forms
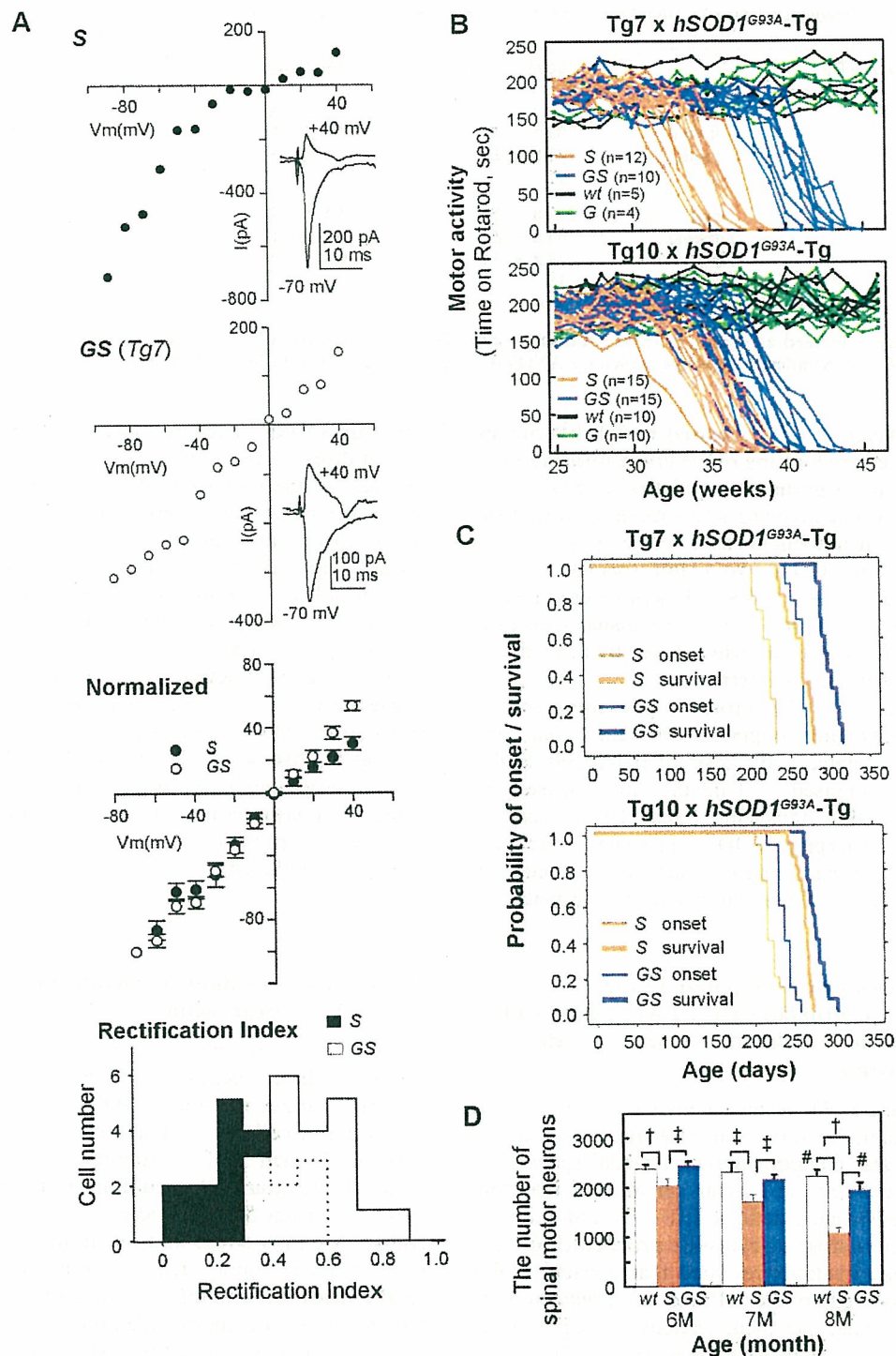
Figure 2. GluR2 overexpression markedly delays disease onset and prolongs survival in $hSOD1^{G93A}$ transgenic mice. (**A**) The majority of AMPA receptors in spinal motoneurons were Ca^{2+}-impermeable in GS (*chat-GluR2/+;hSOD1^{G93A}/+*) littermates, but Ca^{2+}-permeable in S (*hSOD1^{G93A}/+*) littermates. EPSCs of AMPA components were measured from 19 (S, $n = 5$) and 21 (GS, $n = 4$) spinal motoneurons in the same way as in Figure 1E. Rectification index was estimated as 0.321 ± 0.036 for S and 0.535 ± 0.018 for GS (mean $\pm$ SEM, $P < 0.01$). (**B**) GluR2 overexpression delayed the decline of motor performance assessed by the rotarod test. Each point represents the mean of four measurements per day every week on each mouse. Significance of difference in comparison of GS versus S littermates was analyzed by repeated measured ANOVA followed by Fisher's PLSD *post hoc* test (Tg7: $P < 0.0001$ and Tg10: $P = 0.0005$). In both lines, $P < 0.001$ after 32 weeks of age. (**C**) Cumulative probability of disease onset and survival was compared between S and GS littermates. Data were analyzed by Kaplan–Meier life test and log-rank test, and the result is summarized in Table 2. (**D**) Degeneration of spinal motoneurons was significantly delayed by GluR2 overexpression. The 30 μm thick frozen sections were prepared from T10–L5 segments of spinal cords and stained with 0.01% toluidine blue. Large neurons with diameter >25 μm in the ventral horn, which are most severely depleted in $hSOD1^{G93A}$ mice, were counted serially in all sections. Data represent the means $\pm$ SEM from 4–6 mice in each stage. † $P < 0.05$; ‡ $P < 0.01$ and # $P < 0.001$.

Table 2. Prolonging effects of *GluR2* overexpression on the disease onset and survival

chat-GluR2-Tg		$hSOD1^{G93A}/+$	$chat\text{-}GluR2/+, hSOD1^{G93A}/+$	P
Tg7	Onset	219.7 ± 3.0	262.6 ± 2.6	<0.0001
	Survival	262.5 ± 4.5	300.0 ± 3.5	<0.0001
	Length	42.8 ± 2.2	37.9 ± 2.4	0.1563
	n	12	10	
Tg10	Onset	219.8 ± 2.6	238.5 ± 2.7	<0.0001
	Survival	264.5 ± 2.2	279.7 ± 3.1	0.0005
	Length	44.8 ± 2.0	40.8 ± 2.0	0.2189
	n	15	15	

Data are expressed as means ± SEM. Statistical significance in comparison of *hSOD1*/+ (S) and *chat-GluR2*/+ *hSOD1*/+ (GS) littermates was assessed by ANOVA followed by *post hoc* Fisher's PLSD test.

was significantly delayed in GS compared with S littermates. On the other hand, western blotting of the crude mitochondrial fractions revealed that a significant population of SOD1 proteins in this fraction was converted into species distinct from those found in the post-mitochondrial fractions (Fig. 4B). In addition to dimer-sized SOD1, two major species between the monomer and dimer sizes (~25 and 35 kDa) were detected in symptomatic mice. Formation of all the unusual species in crude mitochondrial fractions was also delayed by more than 1 month in GS compared with S littermates.

Certain populations of SOD1 proteins, probably growing aggregates, can be efficiently trapped onto membranes composed of cellulose acetate, and these filter-trapped SOD1 species extensively increased in tandem with disease progression in mutant SOD1 transgenic mice (10). Figure 4C indicates that the filter-trapped SOD1 aggregates were considerably increased during disease onset in S mice, but increased more slowly in GS compared with S littermates.

Unusual SOD1 species first accumulate in the fractions dense with neurofilaments, GFAP, nuclei and mitochondria, which accumulation is markedly delayed by GluR2 overxpression

The finding of unusual SOD1 species depicted in Figure 4 led us to do further subcellular fractionation analysis in order to define in which cellular component such unusual species are localized. We thus divided the lumbar spinal cord into four different organelle-enriched fractions (P1–P4) and a supernatant fraction (S) consisting of cytosolic proteins (Fig. 5A). Immunoblots of these fractions revealed that unusual SOD1 species (*) first appeared in the P1 and P2 fractions long time before disease onset, and then, intensively accumulated into the P1 fraction by the disease onset (Fig. 5B). Nuclei and certain kinds of cytoskeletons such as neurofilaments and glial fibrillary acidic protein (GFAP) were effectively concentrated into the P1 fraction, whereas mitochondria are concentrated into the P2 fraction. In S mice, the dimer-sized species were first detected in the P1 and P2 fractions at 4 months. At 7 months, the stage of disease onset, the P1 fraction contained a considerable amount of unusual SOD1 species of approximately the size of a dimer, 25 and 35 kDa, which were very similar to those detected in the crude mitochondrial fractions as depicted in Figure 4B. These species

were only weakly detected in P2, P3 and P4 fractions at the stage of disease onset, but then accumulated with disease progression. All these unusual SOD1 species were hardly detectable in the cerebrum, cerebellum, testis and muscle from S mice even at end stage (data not shown for cerebellum and muscle), and were hardly detectable in the spinal cord from 9-month-old wt littermates. In GS littermates, dimer-sized species were faintly detected in the P1 and P2 fractions at 6 months of age. Other species accumulated to an enormous extent in the P1 fraction at 8 months of age, the stage of disease onset in GS mice, indicating that the formation of these unusual SOD1 species was delayed concomitantly with the delay of disease onset in GS compared with S littermates. These observations strongly suggest that the misfolding and subsequent conformational changes of mutant SOD1 proteins are delayed when the Ca^{2+}-permeability of AMPA receptors is significantly reduced.

The increase of oxidatively modified proteins is attenuated by GluR2 overexpression

Although the mechanism underlying the marked effects of reduced AMPA receptor Ca^{2+}-permeability on the conformational changes of mutant SOD1 is currently unclear, the attenuation of cellular oxidative stress may be involved. Oxidation of human SOD1 proteins *in vitro* causes cleavage and/or conjugation (33), resulting in the formation of various types of unusual SOD1 species (34,35). Moreover, elevated cellular oxidative stress and resulting oxidative modification of proteins and lipids such as carbonylation are reported in spinal cords from $hSOD1^{G93A}$ mice (36–38). Thus, we compared the level of carbonylated proteins in spinal cord extracts between S and GS littermates, taking it as a marker of cellular oxidative stress. The results in Figure 6 reveal that carbonylated proteins in spinal cords increased only gradually before disease onset, then, increased substantially at disease onset in both S and GS mice. Such drastic increase was not observed in the extracts from cerebrum even in 9-month-old S mice. Statistical analysis revealed that the increase of carbonylation was significantly delayed, by at least 2 months, in GS compared with S littermates. This delay of protein oxidative modification might help explain why conformational changes of SOD1 proteins are delayed in GS mice.
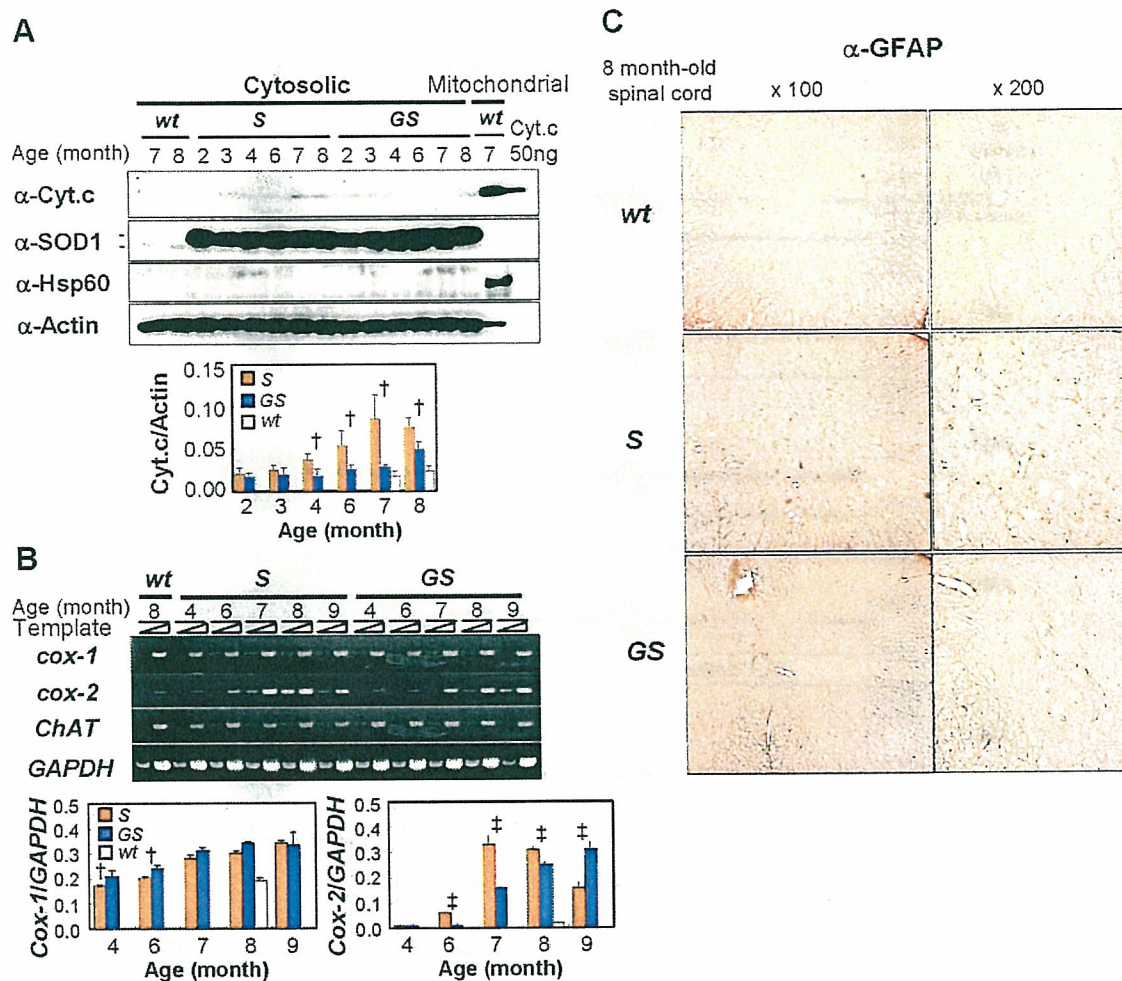
Figure 3. GluR2 overexpression delays cytochrome *c*-release from mitochondria, *cox-2* induction and subsequent astrogliosis. (**A**) Cytochrome *c* release from mitochondria into the cytosol was markedly delayed by GluR2 overexpression. Cytosolic (15 μg) and crude mitochondrial (2 μg) fractions from the lumbar spinal cords were immunoblotted. Hsp60 was used as a marker protein for mitochondria. The anti-SOD1 antibody used in this paper recognizes both human (upper band, 22 kDa) and mouse (lower band, 16 kDa) SOD1. † $P < 0.05$, in comparison of S and GS littermates. (**B**) Induction of *cox-2* transcription was significantly delayed by GluR2 overexpression. RT–PCR analysis was performed using total RNA extracted from lumbar spinal cords. To confirm exponential amplification in each PCR condition, results using two dilution series of template, which differed in concentration by an order of magnitude, are shown. Significance of difference was assessed from the results using larger amounts of templates. † $P < 0.05$ and ‡ $P < 0.01$ (S versus GS). (**C**) Astrogliosis was prominent in 8-month-old S, but was barely detected in GS littermates at the same age. The lumbar regions of mouse spinal cords were immunostained with anti-GFAP antibody.

DISCUSSION

Motoneuronal Ca^{2+}-permeable AMPA receptors contribute to selective cell death in SOD1-related ALS

The present study demonstrates that motoneuronal Ca^{2+}-permeable AMPA receptors contribute to the development of SOD1-related ALS. Reducing permeability by motoneuron-preferential GluR2 overexpression significantly prolongs the lifespan of ALS mice by delaying disease onset (Fig. 2B and C). The mutant SOD1 protein level in the ventral spinal cord was not significantly different between S and GS littermates (Supplementary Material, Fig. S2), and *GluR2* mRNA level in spinal motoneurons did not significantly change during the course of disease in *hSOD1*^{G93A} mice (data not shown). Thus, the beneficial effects of GluR2 overexpression do not result from either a reduction of mutant SOD1 expression or a simple

compensation of decreased GluR2 expression, but from reduced Ca^{2+}-influx through motoneuronal AMPA receptors.

A recent study on chimeric mice between wild-type and mutant SOD1 transgenic mice revealed that the death of motoneurons expressing mutant SOD1 can be delayed when the surrounding non-neuronal cells do not express mutant SOD1 (39). This finding indicates that motoneuronal death triggered by mutant SOD1 is not cell-autonomous, but also depends on the interactions with surrounding glial cells expressing mutant SOD1. However, there must be a reason why only motoneurons die among the neurons surrounded by non-neuronal cells expressing mutant SOD1. The present study provides evidence that the expression of Ca^{2+}-permeable AMPA receptors confers a critical feature on motoneurons such that they undergo death in response to mutant SOD1 effects within themselves and surrounding cells.
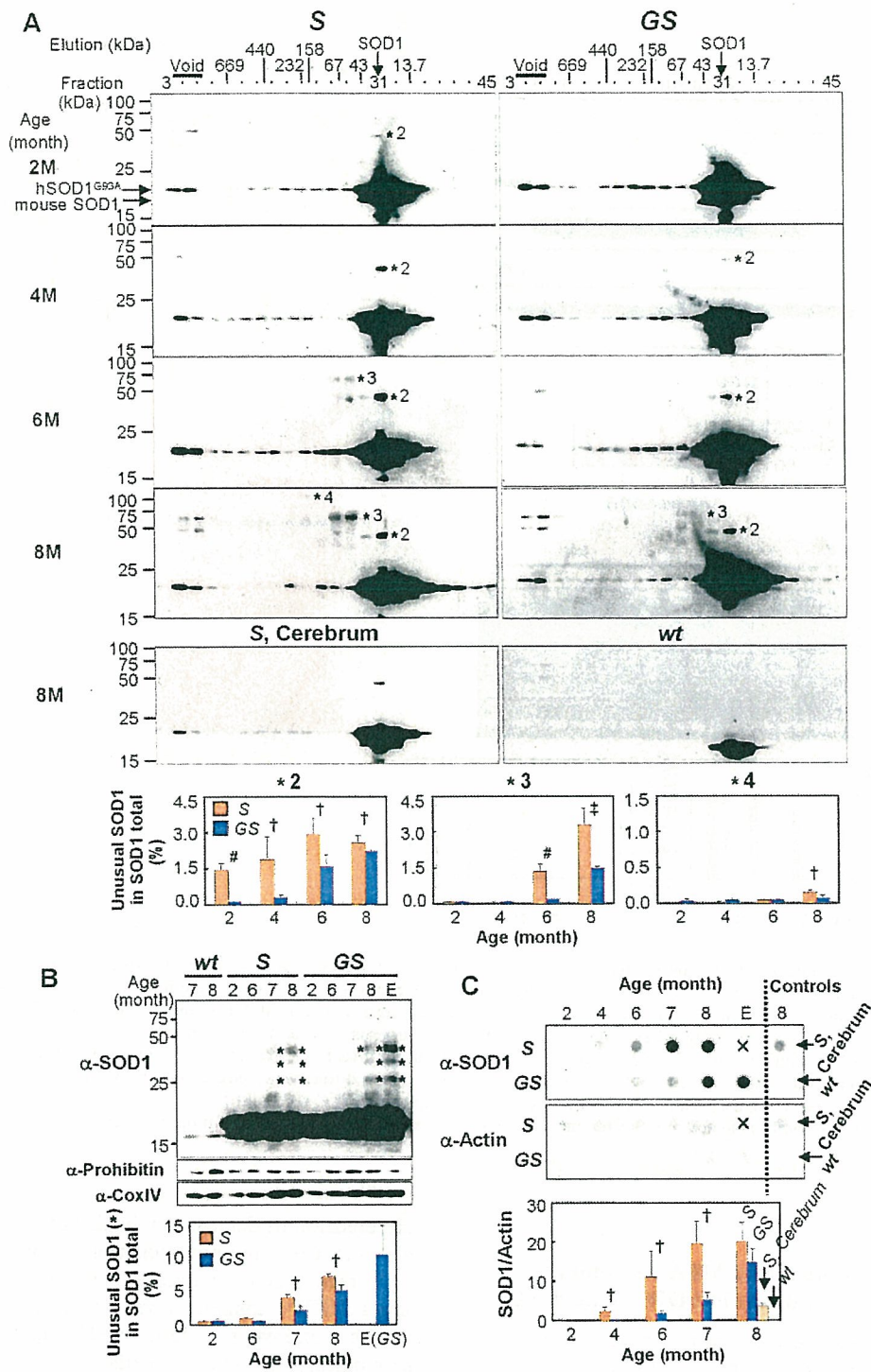
Figure 4. Distinctive patterns of unusual SOD1 species are found in the fractions derived from the cytosol and organelle/cytoskeleton, the formation of which is markedly delayed by GluR2 overexpression. (**A**) A very small population of SOD1 proteins is converted into oligomer-sized species in the cytosol long before disease onset, which was effectively delayed by GluR2 overexpression. HPLC fractions derived from ∼100 μg of post-mitochondrial (cytosolic protein-enriched) fractions were immunoblotted. Formation of unusual SOD1 species corresponding to a dimer (*2), a trimer (*3) and a tetramer (*4) in size was significantly delayed in GS compared with S littermates. † $P < 0.05$, ‡ $P < 0.01$ and # $P < 0.001$. Non-specific bands appear in the void fraction. (**B**) Unusual SOD1 species differing from those in post-mitochondrial fractions were detected in crude mitochondrial (organelle/cytoskeleton-enriched) fractions at disease onset, which was effectively delayed by GluR2 overexpression. The crude mitochondrial fractions (5 μg) were immunoblotted. Asterisks indicate usual SOD1 species corresponding to a dimer, ∼25 and 35 kDa sizes. † $P < 0.05$ (S versus GS littermates). (**C**) Filter-trapped SOD1, which might represent misfolded or aggregated forms, increased markedly before disease onset in S, but very slowly in GS littermates. Aliquots 12.5 μg of the post-mitochondrial fractions were solubilized with TBST (0.025% Tween-20) and filtered using cellulose acetate membrane (0.2 μm diameter) followed by immunostaining (10). † $P < 0.05$ (S versus GS littermates).
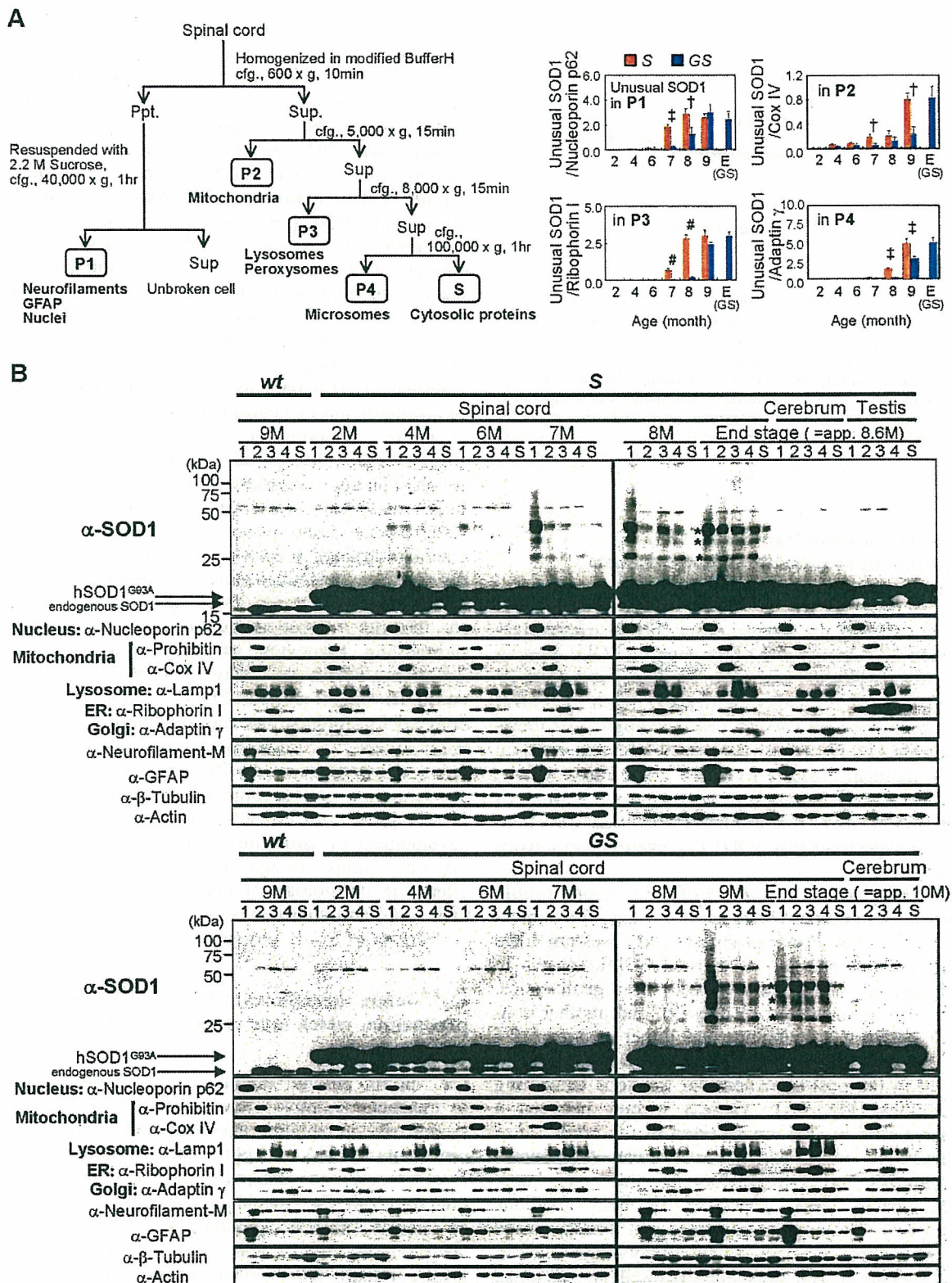
Figure 5. Unusual SOD1 species first appear in the fraction enriched in neurofilaments, GFAP, nuclei and mitochondria, which is markedly delayed by GluR2 overexpression. (**A**) The procedure for subcellular fractionation. The representative organelles and cytoskeletons enriched in each fraction are indicated. (**B**) Unusual SOD1 species (asterisks) were first detected in P1 and P2 before disease onset, and then accumulated in other organelle fractions with disease progression. Aliquots of 5 μg of each fraction was immunoblotted. The distribution of each organelle and cytoskeletons was evaluated using antibodies for each marker protein. Accumulation of unusual SOD1 species in spinal cords was significantly delayed in GS compared with S littermates. † *P* < 0.05, ‡ *P* < 0.01 and # *P* < 0.001 (S versus GS littermates).
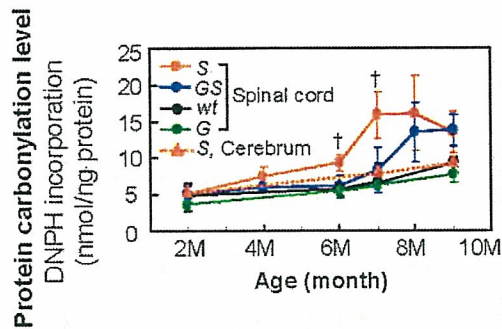
Figure 6. Oxidative modification of proteins is slowly increased by GluR2 overexpression. Tissue extracts were treated with DNPH, which specifically reacted with carbonyl groups in the protein side chains and converted into DNP–hydrazone. The levels of carbonylated proteins in spinal cords, which were evaluated from the absorption of DNP–hydrazone (375 nm), were significantly higher in the 6- and 7-month-old S littermates and 8-month-old GS littermates compared with G and wt littermates ($P < 0.05$). In comparison between the S and GS littermates, the carbonylated protein levels were significantly higher in S than GS littermates at the age of 6 and 7 months († $P < 0.05$). $n = 3$–4 mice per each group.

Ca²⁺-influx though motoneuronal AMPA receptors promotes conversion of SOD1 protein into aberrant forms

In addition to delaying the disease onset, GluR2 overexpression succeeded in delaying the conversion of SOD1 protein into unusual forms (Figs 4 and 5B). To date, more than 20 papers have reported the delay of disease onset in mutant SOD1 transgenic mice by various pharmacological or transgenic techniques (1). However, the effects of such trials on SOD1 conformational changes have yet to be shown. Here, we provide the first evidence that disease onset is delayed when conversion of SOD1 into unusual forms is delayed, consistent with the hypothesis that SOD1 aggregation participates in ALS pathogenesis.

This study also provides an outline of the temporal profile for the formation of unusual SOD1 species during the clinical course of mouse ALS. Previous studies with western blots detected two distinct patterns of unusual SOD1 species in spinal cord extracts from mutant SOD1 transgenic mice. One is a set of oligomer-sized species (9), and another contains species between a monomer and dimer in size (10–12). Here, we show that trimer- and tetramer-sized species are detectable in the post-mitochondrial fractions containing cytosolic proteins (Fig. 4A), whereas species between a monomer and dimer in size are detected in the crude mitochondrial fractions containing major cellular components such as organelles and cytoskeleton. On the other hand, dimer-sized species were detectable in both fractions (Figs 4B and 5B). The amount of trimer and tetramer-sized species in the cytosol seemed comparatively very small to the unusual species in the organelle/cytoskeleton fractions, as these species are no longer detectable in Figure 5B, an experiment in which the same subcellular fraction amounts were loaded to the respective lanes. The first detectable unusual SOD1 species are dimer-sized species that appear several months before disease onset. Subsequently, a very small population of SOD1 proteins grows into trimer- and tetramer-sized species in the cytosol. On the other hand, a large amount of SOD1 protein is converted into ~25 and 35 kDa-sized species. These unusual species first appear in the P1 and P2 fractions and then extensively accumulate into the P1 fraction by disease onset. The presence in the P2 mitochondrial fraction might be related to the dysfunction of mitochondria that has been reported in $hSOD1^{G93A}$ mice around disease onset (1,31). In the P1 fraction, nuclei and certain kind of filamentous cytoskeletons such as neurofilaments and GFAP, but not actin filaments or microtubiles, are effectively concentrated. The extensive accumulation of unusual SOD1 species in the P1 fraction implies that these species are fundamentally associated with neurofilaments or GFAP, because a further fractionation study revealed that these species do not independently accumulate in the nuclei (data not shown). Abnormalities in the neurofilaments observed in ALS patients and mutant SOD1 mice, such as an accumulation of neurofilament inclusions (1) and a defect in axonal transport (4), might be closely related to this phenomenon. Alternatively, those SOD1 species might be involved in aggresome-like structures, as observed in HEK293 cells transfected with G85R and G93A SOD1 mutants (9). After disease onset, unusual species spread to other organelle fractions enriched in lysosomes, peroxysomes and microsomes derived from the endoplasmic reticulum (ER), Golgi apparatus and plasma membrane. These alterations in SOD1 proteins are thought to predominantly occur in motoneurons and surrounding astrocytes, as SOD1-containing proteinacious inclusions, which are likely to have developed from high-molecular-weight-shifted SOD1 species, are specifically detected in motoneurons and neighboring astrocytes in end-stage $hSOD1^{G93A}$ mice (6–8). The reduction of Ca²⁺-influx through motoneuronal AMPA receptors successfully delayed the formation of the entire range of unusual SOD1 species in the spinal cord extracts (Figs 4 and 5A) as well as the development of astrogliosis (Fig. 3C). These results suggest that Ca²⁺-influx through motoneuronal AMPA receptors can affect the physiology of neighboring astrocytes as well as their own, and contributes to the misfolding and subsequent conversion of SOD1 protein.

Ca²⁺-influx through AMPA receptors enhances ROS production, which may induce the misfolding of SOD1 proteins

Ca²⁺-influx through motoneuronal AMPA receptors seems to enhance oxidative stress primarily in motoneurons and secondarily in neighboring astrocytes. Activation of Ca²⁺-permeable AMPA receptors causes rapid increases in the level of cytosolic calcium, which are rapidly attenuated by trapping with Ca²⁺-chelating proteins and by incorporation of calcium into mitochondria and ER (40). As spinal motoneurons are less capable of buffering increased calcium levels, probably due to a lack of major Ca²⁺-chelating proteins such as parvalbumin and calbindin D28K (41), a large proportion of free calcium is reported to be incorporated into mitochondria, resulting in enhanced ROS production (42). Evidence suggests that ROS generated in motoneurons can exit from the motoneurons and cause oxidative disruption of glutamate transporters and increased ROS level in neighboring

astrocytes (43). The loss of astrocytic glutamate transporters, which has been preferentially observed in the affected area in ALS patients and mouse models (15,43,44), accelerates AMPA receptor-mediated Ca^{2+}-influx and ROS generation within motoneurons, resulting in a vicious cycle to enhance the oxidative stress in motoneurons and neighboring astrocytes (45).

Enhanced ROS levels might, in part, account for the formation of unusual SOD1 species, as oxidative modification by ROS has been shown to convert SOD1 proteins into a variety of unusual forms, at least *in vitro* (34,35). We found a good correlation between the levels of carbonylated proteins and unusual SOD1 species in the spinal cord extracts from S and GS mice. Both levels were rapidly increased at disease onset, but these increases were similarly attenuated when the Ca^{2+}-permeability of AMPA receptors was reduced (Figs 4, 5B and 6). This correlation may imply that the increased cellular oxidative stress resulting from activation of motoneuronal Ca^{2+}-permeable AMPA receptors induces the misfolding and subsequent conversion of SOD1 protein within motoneurons and adjacent glial cells.

MATERIALS AND METHODS

The sequence information for the primers and probes is described in Supplementary Material, Table S1. All the data shown are representative of three mice per group when the number of mice (n) used for experiments is not mentioned. Signals in immunoblots and RT–PCR were quantified with NIH image software (1.61J). Statistical significance was assessed by the two-tailed Student's t-test when the statistical method is not mentioned. All protein electrophoreses in this paper utilized SDS–PAGE under reducing conditions. Antibodies were used for immunoblots and immunohistochemistry, which comprised of: anti-SOD1 (Stressgen, SOD-100), anti-GluR2 (BD PharMingen, 556341), anti-ChAT (Chemicon, AB144P), anti-cytochrome *c* (BD PharMingen, 556433), anti-Hsp60 (Sigma, H4149), anti-actin (Chemicon, MAB1501), anti-GFAP (Chemicon, MsX GFAP), anti-prohibitin (NeoMarkers, MS-261-P0), anti-CoxIV (Molecular Probes, A-6431), anti-nucleoporin p62 (BD Transduction Laboratories, N43620), anti-ribophorin I (Santa Cruz, sc-12164), anti-Lamp1 (BD PharMingen, 553792), anti-adaptin gamma (BD Transduction Laboratories, A36120), anti-neurofilament-M (Chemicon, AB1987), and anti-beta-tubulin (Sigma, T 4026) antibodies.

Generation of GluR2 transgenic mice

The transgene construct contained the 6.4 kb promoter region of the mouse *ChAT* gene (AF019045), the 2.6 kb rat *GluR2* coding sequence (CDS, M85035), internal ribosome entry sequence (IRES), *EGFP* CDS and the SV40 polyadenylation signal, in that order. As the *ChAT* promoter region contains an open reading frame of a vesicular acetylcholine transporter (*VAChT*) intronless gene (23), we introduced a stop codon at the 55th amino acid position to avoid producing a functional VAChT protein from this construct. The region from *IRES* to the polyadenylation signal was derived from the pIRES2–EGFP vector (Clonetech), with a base substitution so as to delete a *Not*I site in the *EGFP* 3′-untranslated region.

The *Not*I-digested 10.9 kb DNA fragment was injected into C57BL/6J mouse eggs, and three transgenic lines, Tg3, Tg7 and Tg10, were established.

Taqman quantitative DNA PCR was performed using probe–primer sets specific to *EGFP* and two internal control genes, *SOD1* and *CPTI*, on an ABI7700 thermal cycler (PE Biosystems) under the conditions recommended by the manufacturer. Data were normalized using results from the *EGFP* knock-in mouse in the *Cx43* gene (M. Tanaka and S. Itohara, unpublished data), which displays a single copy of *EGFP* in the genome. Then absolute *EGFP* copy numbers in Tg3 ($n = 3$) Tg7 ($n = 3$) and Tg10 ($n = 5$) of *chat-GluR2* mice were calculated as 2.10 ± 0.04, 9.31 ± 0.14 and 16.44 ± 0.67 copies for the *SOD1* control, and 2.13 ± 0.07, 10.20 ± 0.09 and 16.43 ± 1.28 copies for the *CPTI* control, respectively (mean $\pm$ SD). The transgene copy number was thus represented as the mean of these two values.

Electrophysiological recordings

Electrophysiological experiments were performed as previously described (46) using 200–250 μm slices of spinal cord lumbar regions from mice at the postnatal ages of 4–7 days. Whole-cell patch-clamp recordings were performed with motoneurons identified using biocytin-containing Cs-based intracellular solution. To isolate the AMPA current, the extracellular solution contained 20 μM bicuculline, 25 μM D-2-amino-phosphonovaleric acid (D-APV) and 10 μM strychnine, which blocks the GABA, NMDA and glycine receptors, respectively. A glass electrode containing artificial cerebrospinal fluid positioned in the spinal cord was used for synaptic stimulation.

Quantitative analysis of gene expression levels in motoneurons

Spinal cords from 6–8-month-old mice were dissected without fixation, immediately embedded in OCT compound (Tissue-Tek), and frozen in liquid nitrogen. Frozen sections 30 μm thick were processed and stained using 0.01% toluidine blue, and motoneurons in spinal cords were clipped out of sections using laser microdissection (AS LMD, Leica) according to the manufacturer's protocol. About 1000 clipped slices of motoneurons were collected per mouse and subjected to RNA purification using an RNAeasy kit (Qiagen), followed by cDNA synthesis primed with oligo-dT using Superscript II (Gibco-Brl). The gene expression level was examined by Taqman real-time quantitative PCR using probe–primer sets specific to target genes. PCR was performed on an ABI7700 thermalcycler (PE Biosystems) under the manufacturer's recommended conditions, using cDNA derived from 60 (for *GluR2-4* and *ChAT*) or 10 (for *SOD1* and *GAPDH*) clipped slices of motoneurons as templates. Data were normalized with the expression level of *GAPDH*, and presented as a relative expression level compared with the level in the C57BL/6J non-transgenic control mouse.

Animals

Non-transgenic littermates without any transgene are indicated as wt to distinguish them from non-transgenic control mice,

C57BL/6J mice. All data except for Table 1 and Figure 1E are comparisons among littermates. The G1L line of transgenic mice harboring the G93A-mutated human *SOD1* gene (B6SJL-*TgN(SOD1-G93A)*1Gur^dl) was purchased from Jackson Laboratories and backcrossed with C57BL/6J mice. We used the littermates generated by crossing male *hSOD1*^G93A mice (fourth backcross-generation) with female *chat-GluR2* transgenic mice for all analyses except for a study of disease onset and mortality in Tg10 line (Table 2 and Fig. 2B and C), that involved three S and three GS littermates generated from the third backcrossed *hSOD1*^G93A mouse. To determine the day of disease onset, mice were subjected to the rotarod test (47). The retention time on a rotating wheel, the rotarod score, was measured four times per day with a 1-week interval in a blind fashion. Each trial lasted for a maximum of 5 min, during which time the wheel rotates with a linear acceleration from 4 to 40 rpm. The day of disease onset was defined as the day just before the mean retention time of four trials was sequentially shortened to <80% of the previous time. The end time was defined as the day of death or the day when the mouse was unable to right itself within 30 s (25).

Preparation of crude mitochondrial and post-mitochondrial fractions

Crude mitochondrial and post-mitochondrial fractions were prepared according to an established method (31) with certain modifications. The bovine strum albumin concentration in buffer H was reduced to 0.1%. The spinal cord L1–L5 segments were homogenized in buffer H (1 mg tissue/10 μl buffer H) on ice and centrifuged at 600g for 5 min at 4°C to remove unbroken cells. The supernatant was centrifuged at 13 500g for 10 min at 4°C, dividing into pellet (crude mitochondrial fraction) and supernatant (post-mitochondrial fraction).

Size-exclusive chromatography

Approximately 200 μg of cytosolic extracts were filtered through Millex-HV PVDF filters (Millipore, 0.45 μm diameter), concentrated with a Vivaspin column (Vivascience, cut-off size, MW 10 000), then resolved on a Superdex200 PC3.2/30 column (linear fractionation range, MW 10 000–600 000; bed volume, 2.4 ml; Pharmacia Biotech) at a flow rate of 40 μl/min in 50 mM sodium phosphate with 150 mM NaCl, pH 7.0. Fractionation started when 800 μl was eluted, and a 30 μl/tube of elutant was collected for a total of 48 tubes. Void volume was determined by the elution profile of dextran blue (2000 kDa). The column was calibrated using gel filtration calibration kits for high- and low-molecular weights (Amersham Bioscience).

Subcellular fractionation

Figure 5A represents a schematic of this procedure. Whole spinal cords were gently homogenized in modified buffer H [0.22 M D-mannitol, 0.07 M sucrose, 20 mM HEPES, pH 7.4, 1 mM EGTA and complete protease inhibitor cocktail (Roche), at 1 mg tissue/10 μl buffer] with a glass–Teflon

homogenizer (10 up-and-down strokes) on ice, and centrifuged at 600g for 10 min. The supernatants were sequentially centrifuged at 5000g for 15 min, 8000g for 15 min and 100 000g for 1 h, to obtain three pellets (P2, P3 and P4) and the resulting supernatant (S). The pellets generated by the first brief centrifugation were very gently suspended with 2.2 M sucrose containing complete protease inhibitor cocktail (1 mg starting tissue/15 μl), and centrifuged at 40 000g for 1 h. The resulting pellets (P1) were rinsed with modified buffer H followed by centrifugation at 12 000g for 10 min. The pellets of P1, P2, P3 and P4 were finally resuspended with 1/4, 2, 1/2 and 1/2 volume (μl) of modified buffer H per starting tissue weight (mg), respectively. All centrifugations were performed at 4°C.

Measurement of protein carbonylation

Freshly dissected tissues were sonicated in buffer [50 mM Tris–HCl, pH 7.6, 20 mM Na$_4$P$_2$O$_7$, 20 mM sodium fluoride, 1 mM EGTA, 5 mM EDTA, 5 mM DTT and complete protease inhibitor cocktail (Roche), at 1 mg tissue/20 μl buffer] and centrifuged at 500g for 5 min. The supernatants were further centrifuged at 100 000g for 1 h, and the resulting supernatants were used. The levels of carbonylated proteins in these supernatants were evaluated by measuring absorbance derived from dinitrophenyl (DNP)–hydrazone as previously described (36) with slight modifications. We started with 40 μg of protein and used 6% SOD for a solubilization of the trichloroacetic acid precipitates.

SUPPLEMENTARY MATERIAL

Supplementary Material is available at HMG Online.

ACKNOWLEDGEMENTS

REFERENCES

1. Julien, J.P. (2001) Amyotrophic lateral sclerosis unfolding the toxicity of the misfolded. *Cell*, **104**, 581–591.
2. Rosen, D.R., Siddique, T., Patterson, D., Figlewicz, D.A., Sapp, P., Hentati, A., Donaldson, D., Goto, J., O'Regan, J.P., Deng, H.X. *et al.* (1993) Mutations in Cu/Zn superoxide dismutase gene are associated with familial amyotrophic lateral sclerosis. *Nature*, **362**, 59–62.

3. Gurney, M.E., Pu, H., Chiu, A.Y., Dal Canto, M.C., Polchow, C.Y., Alexander, D.D., Caliendo, J., Hentati, A., Kwon, Y.W., Deng, H.X. *et al.* (1994) Motor neuron degeneration in mice that express a human Cu,Zn superoxide dismutase mutation. *Science*, 264, 1772–1775.

4. Cleveland, D.W. and Rothstein, J.D. (2001) From Charcot to Lou Gehrig: deciphering selective motor neuron death in ALS. *Nat. Rev. Neurosci.*, 2, 806–819.

5. Valentine, J.S. and Hart, P.J. (2003) Misfolded CuZnSOD and amyotrophic lateral sclerosis. *Proc. Natl Acad. Sci. USA*, 100, 3617–3622.

6. Shibata, N., Asayama, K., Hirano, A. and Kobayashi, M. (1996) Immunohistochemical study on superoxide dismutases in spinal cords from autopsied patients with amyotrophic lateral sclerosis. *Dev. Neurosci.*, 18, 492–498.

7. Bruijn, L.I., Houseweart, M.K., Kato, S., Anderson, K.L., Anderson, S.D., Ohama, E., Reaume, A.G., Scott, R.W. and Cleveland, D.W. (1998) Aggregation and motor neuron toxicity of an ALS-linked SOD1 mutant independent from wild-type SOD1. *Science*, 281, 1851–1854.

8. Watanabe, M., Dykes-Hoberg, M., Culotta, V.C., Price, D.L., Wong, P.C. and Rothstein, J.D. (2001) Histological evidence of protein aggregation in mutant SOD1 transgenic mice and in amyotrophic lateral sclerosis neural tissues. *Neurobiol. Dis.*, 8, 933–941.

9. Johnston, J.A., Dalton, M.J., Gurney, M.E. and Kopito, R.R. (2000) Formation of high molecular weight complexes of mutant Cu, Zn-superoxide dismutase in a mouse model for familial amyotrophic lateral sclerosis. *Proc. Natl Acad. Sci. USA*, 97, 12571–12576.

10. Wang, J., Xu, G. and Borchelt, D.R. (2002) High molecular weight complexes of mutant superoxide dismutase 1: age-dependent and tissue-specific accumulation. *Neurobiol. Dis.*, 9, 139–248.

11. Wang, J., Slunt, H., Gonzales, V., Fromholt, D., Coonfield, M., Copeland, N.G., Jenkins, N.A. and Borchelt, D.R. (2003) Copper-binding-site-null SOD1 causes ALS in transgenic mice: aggregates of non-native SOD1 delineate a common feature. *Hum. Mol. Genet.*, 12, 2753–2764.

12. Puttaparthi, K., Wojcik, C., Rajendran, B., DeMartino, G.N. and Elliott, J.L. (2003) Aggregate formation in the spinal cord of mutant SOD1 transgenic mice is reversible and mediated by proteasomes. *J. Neurochem.*, 87, 851–860.

13. Durham, H.D., Roy, J., Dong, L. and Figlewicz, D.A. (1997) Aggregation of mutant Cu/Zn superoxide dismutase proteins in a culture model of ALS. *J. Neuropathol. Exp. Neurol.*, 56, 523–530.

14. Shaw, P.J. and Eggett, C.J. (2000) Molecular factors underlying selective vulnerability of motor neurons to neurodegeneration in amyotrophic lateral sclerosis. *J. Neurol.*, 247 (Suppl. 1), I17–I27.

15. Rothstein, J.D., Van Kammen, M., Levey, A.I., Martin, L.J. and Kuncl, R.W. (1995) Selective loss of glial glutamate transporter GLT-1 in amyotrophic lateral sclerosis. *Ann. Neurol.*, 38, 73–84.

16. Van Damme, P., Leyssen, M., Callewaert, G., Robberecht, W. and Van Den Bosch, L. (2003) The AMPA receptor antagonist NBQX prolongs survival in a transgenic mouse model of amyotrophic lateral sclerosis. *Neurosci. Lett.*, 343, 81–84.

17. Gurney, M.E., Fleck, T.J., Himes, C.S. and Hall, E.D. (1998) Riluzole preserves motor function in a transgenic model of familial amyotrophic lateral sclerosis. *Neurology*, 50, 62–66.

18. Bar-Peled, O., O'Brien, R.J., Morrison, J.H. and Rothstein, J.D. (1999) Cultured motor neurons possess calcium-permeable AMPA/kainate receptors. *Neuroreport*, 10, 855–859.

19. Kruman, II, Pedersen, W.A., Springer, J.E. and Mattson, M.P. (1999) ALS-linked Cu/Zn-SOD mutation increases vulnerability of motor neurons to excitotoxicity by a mechanism involving increased oxidative stress and perturbed calcium homeostasis. *Exp. Neurol.*, 160, 28–39.

20. Hollmann, M. and Heinemann, S. (1994) Cloned glutamate receptors. *Annu. Rev. Neurosci.*, 17, 31–108.

21. Sommer, B., Kohler, M., Sprengel, R. and Seeburg, P.H. (1991) RNA editing in brain controls a determinant of ion flow in glutamate-gated channels. *Cell*, 67, 11–19.

22. Kawahara, Y., Ito, K., Sun, H., Aizawa, H., Kanazawa, I. and Kwak, S. (2004) Glutamate receptors: RNA editing and death of motor neurons. *Nature*, 427, 801.

23. Naciff, J.M., Behbehani, M.M., Misawa, H. and Dedman, J.R. (1999) Identification and transgenic analysis of a murine promoter that targets cholinergic neuron expression. *J. Neurochem.*, 72, 17–28.

24. Tateno, M., Fukunishi, Y., Komatsu, S., Okazaki, Y., Kawai, J., Shibata, K., Itoh, M., Muramatsu, M., Held, W.A. and Hayashizaki, Y. (2001) Identification of a novel member of the snail/Gfi-1 repressor family, mlt 1, which is methylated and silenced in liver tumors of SV40 T antigen transgenic mice. *Cancer Res.*, 61, 1144–1153.

25. Li, M., Ona, V.O., Guegan, C., Chen, M., Jackson-Lewis, V., Andrews, L.J., Olszewski, A.J., Stieg, P.E., Lee, J.P., Przedborski, S. *et al.* (2000) Functional role of caspase-1 and caspase-3 in an ALS transgenic mouse model. *Science*, 288, 335–339.

26. Zhu, S., Stavrovskaya, I.G., Drozda, M., Kim, B.Y., Ona, V., Li, M., Sarang, S., Liu, A.S., Hartley, D.M., Wu du, C. *et al.* (2002) Minocycline inhibits cytochrome c release and delays progression of amyotrophic lateral sclerosis in mice. *Nature*, 417, 74–78.

27. Drachman, D.B., Frank, K., Dykes-Hoberg, M., Teismann, P., Almer, G., Przedborski, S. and Rothstein, J.D. (2002) Cyclooxygenase 2 inhibition protects motor neurons and prolongs survival in a transgenic mouse model of ALS. *Ann. Neurol.*, 52, 771–778.

28. van Gurp, M., Festjens, N., van Loo, G., Saelens, X. and Vandenabeele, P. (2003) Mitochondrial intermembrane proteins in cell death. *Biochem. Biophys. Res. Commun.*, 304, 487–497.

29. Bezzi, P., Carmignoto, G., Pasti, L., Vesce, S., Rossi, D., Rizzini, B.L., Pozzan, T. and Volterra, A. (1998) Prostaglandins stimulate calcium-dependent glutamate release in astrocytes. *Nature*, 391, 281–285.

30. Hall, E.D., Oostveen, J.A. and Gurney, M.E. (1998) Relationship of microglial and astrocytic activation to disease onset and progression in a transgenic model of familial ALS. *Glia*, 23, 249–256.

31. Mattiazzi, M., D'Aurelio, M., Gajewski, C.D., Martushova, K., Kiaei, M., Beal, M.F. and Manfredi, G. (2002) Mutated human SOD1 causes dysfunction of oxidative phosphorylation in mitochondria of transgenic mice. *J. Biol. Chem.*, 277, 29626–29633.

32. Okado-Matsumoto, A. and Fridovich, I. (2001) Subcellular distribution of superoxide dismutases (SOD) in rat liver: Cu,Zn-SOD in mitochondria. *J. Biol. Chem.*, 276, 38388–38393.

33. Ookawara, T., Kawamura, N., Kitagawa, Y. and Taniguchi, N. (1992) Site-specific and random fragmentation of Cu,Zn-superoxide dismutase by glycation reaction. Implication of reactive oxygen species. *J. Biol. Chem.*, 267, 18505–18510.

34. Urushitani, M., Kurisu, J., Tsukita, K. and Takahashi, R. (2002) Proteasomal inhibition by misfolded mutant superoxide dismutase 1 induces selective motor neuron death in familial amyotrophic lateral sclerosis. *J. Neurochem.*, 83, 1030–1042.

35. Rakhit, R., Cunningham, P., Furtos-Matei, A., Dahan, S., Qi, X.F., Crow, J.P., Cashman, N.R., Kondejewski, L.H. and Chakrabartty, A. (2002) Oxidation-induced misfolding and aggregation of superoxide dismutase and its implications for amyotrophic lateral sclerosis. *J. Biol. Chem.*, 277, 47551–47556.

36. Andrus, P.K., Fleck, T.J., Gurney, M.E. and Hall, E.D. (1998) Protein oxidative damage in a transgenic mouse model of familial amyotrophic lateral sclerosis. *J. Neurochem.*, 71, 2041–2048.

37. Liu, R., Althaus, J.S., Ellerbrock, B.R., Becker, D.A. and Gurney, M.E. (1998) Enhanced oxygen radical production in a transgenic mouse model of familial amyotrophic lateral sclerosis. *Ann. Neurol.*, 44, 763–770.

38. Liu, D., Wen, J., Liu, J. and Li, L. (1999) The roles of free radicals in amyotrophic lateral sclerosis: reactive oxygen species and elevated oxidation of protein, DNA, and membrane phospholipids. *FASEB J.*, 13, 2318–2328.

39. Clement, A.M., Nguyen, M.D., Roberts, E.A., Garcia, M.L., Boillee, S., Rule, M., McMahon, A.P., Doucette, W., Siwek, D., Ferrante, R.J. *et al.* (2003) Wild-type nonneuronal cells extend survival of SOD1 mutant motor neurons in ALS mice. *Science*, 302, 113–117.

40. Orrenius, S., McConkey, D.J., Bellomo, G. and Nicotera, P. (1989) Role of Ca^{2+} in toxic cell killing. *Trends Pharmacol. Sci.*, 10, 281–285.

41. Alexianu, M.E., Ho, B.K., Mohamed, A.H., La Bella, V., Smith, R.G. and Appel, S.H. (1994) The role of calcium-binding proteins in selective motoneuron vulnerability in amyotrophic lateral sclerosis. *Ann. Neurol.*, 36, 846–858.

42. Carriedo, S.G., Sensi, S.L., Yin, H.Z. and Weiss, J.H. (2000) AMPA exposures induce mitochondrial Ca(2+) overload and ROS generation in spinal motor neurons *in vitro*. *J. Neurosci.*, 20, 240–250.

43. Rao, S.D., Yin, H.Z. and Weiss, J.H. (2003) Disruption of glial glutamate transport by reactive oxygen species produced in motor neurons. *J. Neurosci.*, 23, 2627–2633.

44. Bendotti, C., Tortarolo, M., Suchak, S.K., Calvaresi, N., Carvelli, L., Bastone, A., Rizzi, M., Rattray, M. and Mennini, T. (2001) Transgenic SOD1 G93A mice develop reduced GLT-1 in spinal cord without alterations in cerebrospinal fluid glutamate levels. *J. Neurochem.*, **79**, 737–746.

45. Rao, S.D. and Weiss, J.H. (2004) Excitotoxic and oxidative cross-talk between motor neurons and glia in ALS pathogenesis. *Trends Neurosci.*, **27**, 17–23.

46. Suzuki, T., Miura, M., Nishimura, K. and Aosaki, T. (2001) Dopamine-dependent synaptic plasticity in the striatal cholinergic interneurons. *J. Neurosci.*, **21**, 6492–6501.

47. Inoue, H., Tsukita, K., Iwasato, T., Suzuki, Y., Tomioka, M., Tateno, M., Nagao, M., Kawata, A., Saido, T.C., Miura, M. *et al.* (2003) The crucial role of caspase-9 in the disease progression of a transgenic ALS mouse model. *EMBO J.*, **22**, 6665–6674.

COMPARATIVE STUDY OF GENE EXPRESSION OF CHOLINERGIC SYSTEM-RELATED MOLECULES IN THE HUMAN SPINAL CORD AND TERM PLACENTA

Y. ODA,[ab*] Y. MUROISHI,[ab] H. MISAWA[c] AND S. SUZUKI[d]

[a]*Pathology Laboratory, ALP Company, Limited, 309 Chikaoka-machi, Kanazawa, Ishikawa 920-8217, Japan*

[b]*Department of Molecular and Cellular Pathology, Graduate School of Medical Science, Kanazawa University, Ishikawa, Japan*

[c]*Department of Neurology, Tokyo Metropolitan Institute for Neuroscience, Tokyo, Japan*

[d]*First Department of Pathology, School of Medicine, Yamanashi University, Yamanashi, Japan*

Abstract —By reverse transcription–polymerase chain reaction, Southern blot analysis, direct sequencing, and immunohistochemistry, we studied the expression of cholinergic neuronal markers (choline acetyltransferase [ChAT], vesicular acetylcholine transporter [VAChT], and a high-affinity choline transporter [CHT1]), and gene regulatory molecules (repressor element-1 silencing transcription factor/neuron-restrictive silencer factor [REST/NRSF] and CoREST) in the human spinal cord and term placenta, both of which are well known to contain cells synthesizing acetylcholine. H-type, M-type, N2-type, and R-type ChAT mRNAs, VAChT mRNA, and CHT1 mRNA were detected in the spinal cord, but only H-type, M-type, and N2-type ChAT mRNAs, in the term placenta. REST/NRSF and CoREST were detected in the spinal cord and the placenta, but the amounts of both mRNAs were greater in the placenta than in the spinal cord. Further microdissection analyses revealed that the placental trophoblastic cells contained more REST/NRSF and CoREST transcripts than the spinal large motor neurons. Large motor neurons in the anterior horn of the spinal cord were immunohistochemically stained for ChAT and VAChT. In the placenta, stromal fibroblasts, endothelial cells, and trophoblastic cells of the chorionic villi were positively stained with anti-ChAT antibody but not with anti-VAChT antibody. These findings suggest that transcriptions of the R-type ChAT and VAChT mRNAs are coordinately suppressed in the human term placenta, which might be regulated in part by a REST/NRSF complex that binds to a consensus sequence of repressor element 1/neuron-restrictive silencer element (RE1/NRSE) in the 5′ region upstream from exon R, whereas transcriptions of the H-type, M-type, and N2-type ChAT mRNAs might be independent of control by RE1/NRSE. It is possible that at least two separate regulatory mechanisms of gene expression are present for the human cholinergic gene locus, which might be selected by different combinations of DNA motifs and binding proteins to function in neuronal and non-neuronal cells. © 2004 IBRO. Published by Elsevier Ltd. All rights reserved.

Key words: choline acetyltransferase, CoREST, repressor element 1/neuron-restrictive silencer element, repressor element 1-silencing transcription factor/neuron-restrictive silencer factor, vesicular acetylcholine transporter.

Acetylcholine (ACh) is synthesized from choline and acetyl coenzyme A by the enzyme choline acetyltransferase (ChAT) in the cytoplasm of cholinergic nerve terminals, and is then translocated into synaptic vesicles by the vesicular ACh transporter (VAChT; Oda, 1999). Choline is recruited by being taken up from extracellular fluid by a high-affinity choline transporter (CHT1) in the cholinergic neurons (Okuda et al., 2000). These molecules, ChAT, VAChT, and CHT1, are essential for the ACh neurotransmission of cholinergic neurons. Over the last decade, the gene structures and regulation mechanisms of the gene expression of these three molecules have been scrutinized in several mammalian species, as well as *Drosophila* and *Caenorhabditis*. For example, the genes of ChAT and VAChT are organized into a 'cholinergic gene locus,' where the first intron of the ChAT gene encompasses the open reading frame encoding VAChT (Benjanin et al., 1994; Erickson et al., 1994; Roghani et al., 1994). The expressions of the two molecules are coordinately regulated by multiple regulatory elements, such as cholinergic differentiation factor/leukemia inhibitory factor, ciliary neurotrophic factor, cAMP, and retinoids, in cholinergic neurons (Berrard et al., 1995; Berse and Blusztajn, 1995; Misawa et al., 1995). More recently, the gene encoding CHT1 has been cloned and the biological characteristics of the molecule have been clarified (Apparsundaram et al., 2000; Okuda et al., 2000; Okuda and Haga, 2000).

Syntheses of the cholinergic neuron-essential molecules involved in ACh neurotransmission are elaborately controlled by DNA regulatory elements and the DNA binding proteins. For example, *in vitro* expression studies using rodent cell lines have indicated that nuclear proteins, including repressor element 1-silencing transcription factor/neuron-restrictive silencer factor (REST/NRSF), bind to rat repressor element 1/neuron-restrictive silencer element (RE1/NRSE), which is located upstream of exon R of ChAT, to repress both the R-type of ChAT and VAChT in non-neuronal cells (Lönnerberg et al., 1996; De Gois et al., 2000). The human cholinergic gene locus contains a sequence homologous to rat RE1/NRSE in a corresponding

*Correspondence to: Y. Oda, Pathology Laboratory, ALP Company, Limited, 309 Chikaoka-machi, Kanazawa, Ishikawa 920-8217, Japan. Tel: +81-76-237-4230; fax: +81-76-237-8027.
E-mail address: oda-y@alp-grp.jp (Y. Oda).
Abbreviations: ACh, acetylcholine; BSA, bovine serum albumin; ChAT, choline acetyltransferase; CHT1, high-affinity choline transporter; EDTA, ethylenediaminetetraacetic acid; PBS, phosphate-buffered saline; RE1/NRSE, repressor element 1/neuron-restrictive silencer element; REST/NRSF, repressor element 1-silencing transcription factor/neuron-restrictive silencer factor; RT-PCR, reverse transcription–polymerase chain reaction; TPBS, phosphate-buffered saline containing 0.05% Tween-20; VAChT, vesicular acetylcholine transporter.

Table 1. PCR primers amplifying ChAT, VAChT, CHT1, REST/NRSF, CoREST, β2-microglobulin, and β-actin mRNAs, and the product lengths

Genes		Primers	Product lengths, bp
ChAT			
R-type			
	F	5′-ACACTCCTGAGTGGTGCGGTG-3′	160
	R	5′-TTTTCCAGGATGGGCGTCTTG-3′	
N-type*			
	F	5′-GAGAAAGGAGTAGGAGCCTAG-3′	131 (N2)/303 (N1)
	R	5′-TTTTCCAGGATGGGCGTCTTG-3′	
M-type			
	F	5′-TCAACGCCGCTCTGGGGAC-3′	112
	R	5′-TTTTCCAGGATGGGCGTCTTG-3′	
H-type			
	F1	5′-ATGCATTCCTTTCCCTCCACCAACG-3′	190
	R	5′-ACTGCTGGGAGTTTTTGCTGCCATC-3′	
	F2	5′-TTCACCCTACTCCACACCAGAGATG-3′	154
	R	5′-ACTGCTGGGAGTTTTTGCTGCCATC-3′	
VAChT			
	F	5′-CCTGGCTGCCGGCCTTCGTG-3′	300
	R	5′-AATAGGAGATGTCGGCGATG-3′	
CHT1			
	F1	5′-AAGCCATCATAGTTGGTGGCCGAG-3′	134
	R1	5′-CCAAGCTAGGCCATTACCTGGTAC-3′	
	F2	5′-AAGCCATCATAGTTGGTGGCCGAG-3′	97
	R2	5′-GCTGTGCCATTGATATACCCTCCT-3′	
REST/NRSF**			
	F1	5′-CTCAGAAGACTCATCTAACTAGAC-3′	84/88 (N4)/146 (N62)
	R1	5′-AGGCCACATAACTGCACTGATCAC-3′	
	F2	5′-GACTCATCTAACTAGACATATGCG-3′	81/85 (N4)/143 (N62)
	R2	5′-ATTAGAGGCCACATAACTGCACTG-3′	
CoREST			
	F1	5′-GAGGCAAATGGAAACAATCCC-3′	91
	R1	5′-CCTGAGGAACTGTCTCAGTAG-3′	
	F2	5′-ACGTTGGACTACAGAAGAGCAG-3′	89
	R2	5′-TCCCAATCACGTCTGAGATTGC-3′	
β2-microglobulin			
	F	5′-ACCCCCACTGAAAAAGATGA-3′	114
	R	5′-ATCTTCAAACCTCCATGATG-3′	
β-actin			
	F	5′-ATCTGGCACCACACCTTCTACAATGAGCTGCG-3′	838
	R	5′-CGTCATACTCCTGCTTGCTGATCCACATCTGC-3′	

* And **: splicing variants are in parentheses.
* Misawa et al. (1997) ** Palm et al. (1999)
F, forward; R, reverse.

al. (1997) with some modifications. Briefly, the 5′-region of H-type, M-type, N-type, and R-type ChAT mRNA sequences were amplified with the first strand cDNA generated from the samples for 20, 25, 28, 31, and 34 cycles. One picogram of pBluescript (Stratagene, La Jolla, CA, USA) carrying each type of ChAT cDNAs was used as a control. After amplification, 10 μl of PCR products were electrophoresed on an agarose gel, transferred onto a nylon membrane, and hybridized with a ^{32}P-labeled probe (5′-TGCAGGGAT-GCAGAGGTGTGGA-3′), which could detect all types of the ChAT PCR products. The hybridized signals were densitometrically analyzed with an image analysis software NIH Image 1.61 (NIH, Bethesda, MD, USA). The intensity of the positive bands was measured, and the values of the ChAT bands that were generated with total RNAs extracted from the spinal cord or placenta tissue were normalized to those of the corresponding bands that were generated with 1 pg of the control plasmids.

To examine whether REST/NRSF contains exon N between exons V and VI (Palm et al., 1999), the nucleotide sequence of the PCR products was determined in both directions by cycle-se-

quencing using a dye terminator cycle sequencing kit (Perkin-Elmer Corporation, Foster City, CA, USA).

Experiments for the detection of ChAT mRNAs by Southern blot following RT-PCR, VAChT mRNA by RT-PCR and CHT1 by RT-PCR were performed simultaneously for all tissue samples in the same conditions, and repeated twice. Amplifications of REST/NRSF, CoREST, β-actin, and β2-microglobulin mRNAs by RT-PCR were performed simultaneously for all tissue samples in the same conditions. For relative quantification of REST/NRSF and CoREST transcriptions in the human spinal cord and term placenta, the specific PCR bands of the agarose gel were densitometrically analyzed with an image analysis software NIH Image 1.61. The intensity of the PCR bands was measured, and the values of the REST/NRSF bands (33-cycle PCR with total RNAs extracted from spinal cord or placenta tissue and a set of REST/NRSF F2 and R2 primers; 38-cycle PCR with total RNAs extracted from spinal motor neurons or placental trophoblastic cells and a set of REST/NRSF F2 and R2 primers) or the CoREST bands (33-cycle PCR with total RNAs extracted from spinal cord or